地質調査研究報告

BULLETIN OF THE GEOLOGICAL SURVEY OF JAPAN

概報

表紙の写真

レーザーアブレーション ICP-MS で分析した単斜輝石

　地質調査総合センター 共同利用実験室設置のレーザーアブレーション誘導結合プラズマ質量分析計（LA-ICP-MS）によって局所分析を行った単斜輝石．円形の孔がレーザーアブレーションシステムでアブレートしたクレーターで，大きいものから順に直径は100, 40, 20 μm．淡緑褐色でクレーターのある部分が単斜輝石で，白色（透明）部分が斜長石．写真の長辺は約0.8 mm．

（写真・文：山崎　徹）

Cover photograph

Photomicrograph of craters after laser ablation of clinopyroxene

　Photomicrograph shows craters（100, 40 and 20 μm in decreasing order of size）after laser ablation of clinopyroxene（open Nicol）using laser ablation-inductively coupled plasma-mass spectrometer（LA-ICP-MS）at GSJ-Lab. Pale-greenish brown portion with craters is clinopyroxene and whitish（transparent）portion is plagioclase. Field of view = 0.8 mm.

（Photograph and Caption by Toru Yamasaki）

Report

Multiple trace element analyses for silicate minerals and glasses by laser ablation-inductively coupled plasma-mass spectrometry (LA-ICP-MS)

Toru Yamasaki[1,*], Kohei Yamashita[1,2], Masatsugu Ogasawara[1] and Genji Saito[3]

Abstract: Programs were established in the shared research facilities of the Geological Survey of Japan (GSJ-Lab) for trace element analysis of silicate minerals and glasses in microspots using laser ablation-inductively coupled plasma-mass spectrometry (LA-ICP-MS). National Institute of Standards and Technology (NIST) synthetic glasses reference materials (NIST 613 and NIST 611) were used as external calibration standards, and suitable instrumental operation settings were set as follows; 0.5 L min^{-1} He carrier gas flow rate, 100 μm laser spot diameter, 5 Hz repetition rate, and 40 % laser energy (fluence *ca.* 2.0 J cm^{-2}). NIST 615 and NIST 613 were analyzed as unknown samples to evaluate precision and accuracy. Precision was mostly less than 30 % for 45 elements from ^{45}Sc to ^{238}U for laser spot diameters ranging from 100 to 10 μm. Accuracy was evaluated according to the difference (DIF) between the analytical results and reference values in the literature. Accuracy for the analysis of NIST 613 was DIF < 30 %, except for Sc, Mn, Ni, and Ge. For NIST 615, DIF was less than 30 %, except for Tl with laser spot diameters of 20 and 10 μm, and for Cd with a laser spot diameter of 20 μm. The depths of laser pits for generic conditions for the analysis of clinopyroxene, amphiboles and plagioclase were estimated as extents without penetration of the thin section samples. Two suites of analytical programs (34 and 27 elements) were additionally prepared for general purpose petrological and geochemical discussion and the accuracy of both was evaluated. The DIFs for the suite of 34 elements were mostly less than 30 %, although some for Cr, Mn, Ni, and Cs with laser spot diameters < 40 μm exceeded 30 %. In the suite of 27 elements, the DIFs were < 30 %, except for Sc.

Keywords: Trace elements, Laser Ablation-Inductively Coupled Plasma-Mass Spectrometry (LA-ICP-MS), NIST reference materials

1. Introduction

Since the 1980s, the inductively coupled plasma-mass spectrometry (ICP-MS) technique was actively used as an analytical method for rapid simultaneous multi-element analysis with high sensitivity and a wide dynamic range for analyses of geologic samples (e.g., Houk *et al.*, 1980; Date and Gray, 1985; Hirata *et al.*, 1988; Eggins *et al.*, 1997). Instruments equipped with quadrupole mass filters are the most commonly used in geochemical analyses today. There are two quantitative analytical methods by ICP-MS based on the difference in the introduction of samples, i.e., the solution and laser ablation methods. In

the solution method, geologic samples are firstly decomposed by strong acid(s), diluted with aqueous nitric acid solution by several thousand times, and then introduced to the ICP-MS instrument. The laser ablation method directly introduces an aerosol ablated by a laser to the ICP-MS, and this method enables microspot trace element analysis of samples such as minerals (e.g., Perkins *et al.*, 1993; Fryer *et al.*, 1995; Ludden *et al.*, 1995; Hirata and Kon, 2008, and references therein).

While the solution method is available to perform trace element analysis of minerals by mineral separation from rock samples and subsequent acid digestion, the laser ablation method enables the compositional heterogeneity in a single crystal and

[1] AIST, Geological Survey of Japan, Research Institute of Geology and Geoinformation

[2] Department of Natural History Sciences, Graduate School of Science, Hokkaido University

[3] AIST, Geological Survey of Japan, Research Institute of Earthquake and Volcano Geology

[*] Corresponding author: T. Yamasaki, Central 7, 1-1-1 Higashi, Tsukuba, Ibaraki 305-8567, Japan. Email: t.yamasaki@aist.go.jp

crystal by crystal within a thin section to be evaluated by local analysis. In addition, the laser ablation method has several advantages such as ease of analysis for acid-resistant minerals, smaller effect of interference elements due to absence of oxide production from dissolution in acid, and negligible errors that are unavoidable in the preparation and dilution of solutions (e.g., Kimura *et al*., 1996; Satoh *et al*., 2001).

The stability of a short-term (few milliseconds to seconds) ICP-ion source is generally not good; therefore, a long integration time is required to improve precision for the quadrupole mass filter which scans the target mass range (Kimura *et al*., 1996). Thus, the precision of the solution method is better than the laser ablation method because samples introduced with the solution method are stable for a longer time than with the laser ablation method. The laser ablation method is possibly accompanied by attenuation of the signal intensity by the formation of craters and/or fluctuation of signal intensity due to unstable sample introduction. These observations suggest that the stable introduction of a homogeneous aerosol into ICP-MS is important to improve the precision of the laser ablation method.

Trace element analysis generally requires careful treatment of samples during preparation and analysis. For the solution method, expertise and technique are required for solution preparation in a clean environment, prevention of contamination until introduction to the ICP-MS, and management of the instrument operating conditions during analysis. In contrast, because laser ablation method directly ablates the solid sample, contamination is less problematic. It is possible to obtain stable data of constant quality without expertise for instrumental operation when the laser ablation settings and instrumental analytical conditions for various multipurpose samples are optimized.

The shared research facilities of the Geological Survey of Japan, National Institute of Advanced Science and Technology (GSJ-Lab, AIST) are used as a cooperative managing analytical laboratory for common basic analyses in geological studies (e.g., Ogasawara, 2013a,b). With such analytical instruments, it is important that simple and clear analytical protocols and hardware systems are established for users with various specialties, and such users should understand the precision, accuracy, and limitations of instruments used. In this study, we report on the analytical program and its precision and accuracy for the measurement of multiple trace element compositions covering the mass range from ^{45}Sc to ^{238}U in small spot (100 – 20 μm diameter) on thin (*ca*. 30 μm) layers of geologic samples using LA-ICP-MS at GSJ-Lab. The method in this study aims to establish the simplest multipurpose analytical program to obtain data of multiple trace element compositions with adequate quality for geologic discussion. Thus, it is assumed that focus on specific geochemical purposes with more precise analytical programs would be prepared and reported separately.

2. Experimental conditions

We firstly summarize common instrumentation and operating conditions for the various examinations discussed here, and then describe results for examination of the He carrier gas flow rate and laser ablation conditions in later sections.

2.1 Instrument

The LA-ICP-MS system at the GSJ-Lab consists of a New Wave Research NWR213 laser ablation system coupled to an Agilent 7700 x quadrupole ICP-MS. The laser ablation system consists of a Nd:YAG laser that generates an output wavelength of 213 nm and a maximum pulse energy (fluence) of >30 J cm^{-2}. The diameter of the ablation spot can be varied from 110 to 4 μm, which is controlled by rotating aperture that strips out part of the beam. The sample chamber is 100 × 100 mm^2 and 30 mm deep, and is equipped with a Two Vol ablation cell. The large sample chamber allows 5 normal thin sections and external reference glasses to be loaded and analyzed in a single uninterrupted session.

Argon (Ar) gas is used to plasma, auxiliary and nebuliser (carrier) gas. Helium (He) gas is used to flush the ablated material out of the laser cell, and is then mixed with Ar gas just before entry into the ICP-MS. Thus, nebuliser gas flow is independent of ablation of target materials and transport of aerosol. Recent high-sensitivity analyses in previous studies adopt Ar nebuliser and He carrier gas flow rate as follows: 1.16 L min^{-1} Ar, 0.2 L min^{-1} He (Morishita *et al*., 2005); 0.9 – 1.25 L min^{-1} Ar, 0.3 L min^{-1} He (Eggins and Shelley, 2002); 0.8 L min^{-1} Ar, 0.7 L min^{-1} He (Regnery *et al*., 2009). Flow rates of nebuliser gas and He carrier gas correlate with sampling depth and radio-frequency wave (RF) power in the ICP-MS, and finally, affect the sensitivity. In general, increasing the injection gas (nebuliser and He carrier gas) flow rate results in lowering the plasma temperature and thus debasement of sensitivity in case of a hot-plasma condition. However, in case of cool-plasma condition in this study, those decreasing temperature is not serious problem because originally intended for low-plasma temperature and low-RF power. In addition, RF power to maintain the cool-plasma condition is automatically controlled in the Agilent 7700 x. Therefore, based on previous studies, it can be considered that Ar nebulizer gas flow rates of 0.8 – 1.16 L min^{-1} does not substantially affect to analytical precision under the 1.2 – 1.55 L min^{-1} injection gas flow rate, even if we take account of hardware difference in each instruments. On the other hand, since parameters relevant to final analytical precision are associated with each other, fixation of some parameters is required to evaluation of final

Table 1   LA-ICP-MS operating parameters.

a) Basic operating parameters

Laser	New Wave NWR213
	Nd:YAG Laser
Wavelength	213 nm
Maximum pulse energy	>30 J cm^{-2} (Fluence)
Spot sizes	110–4 μm (apertue system)
ICP-MS	Agilent 7700x
Forward power	1550 W
Nebuliser gas flow	1.03 L min^{-1} (Ar)
Plasma gas flow	15 L min^{-1}
Cones	Ni sample cone
	Ni skimmer cone

b) Summary of analytical conditions of LA system

Laser He carrier gas flow	0.5 L min^{-1}
Laser pulse repetition rate	5 Hz (continuous Z–focus on)
Laser energy for calibration stdandard	40% (Fluence 2.0 J cm^{-2})
Laser spot size for calibration standard	100 μm
Laser warm–up & waiting time	8 seconds

Table 2   Analyte elements, isotopes, dwell time per element.

Element	Mass number	Dwell Time (sec.)
Ca	42	0.1
Sc	45	0.1
Ti	47	0.3
V	51	0.3
Cr	53	0.25
Mn	55	0.1
Co	59	0.25
Ni	60	0.25
Cu	63	0.25
Zn	66	0.25
Ga	69	0.25
Ge	72	0.1
As	75	0.25
Rb	85	0.25
Sr	88	0.25
Y	89	0.25
Zr	90	0.25
Nb	93	0.25
Mo	95	0.25
Cd	111	0.25
Sn	118	0.25
Sb	121	0.25
Cs	133	0.1
Ba	137	0.4
La	139	0.25
Ce	140	0.25
Pr	141	0.25
Nd	146	0.25
Sm	147	0.25
Eu	153	0.25
Gd	157	0.3
Tb	159	0.25
Dy	163	0.4
Ho	165	0.4
Er	166	0.4
Tm	169	0.4
Yb	172	0.3
Lu	175	0.3
Hf	178	0.3
Ta	181	0.3
W	182	0.3
Tl	205	0.3
Pb	208	0.3
Bi	209	0.3
Th	232	0.3
U	238	0.3

analytical precision. For above reasons, we fixed Ar nebuliser gas flow rate as 1 L min^{-1}. This value is an intermediate value of previous studies and had been confirmed by solution method as optimal condition in advance of this study. In the meantime, previous studies adopted wide range of He carrier gas flow rate (0.2 – 0.7 L min^{-1}). Because He carrier gas flow rate relates to ablation of target materials and efficient transport of aerosol, it is considered that effect for final analytical precision is easily affected by hardware system such as ablation cell. Thus we evaluate appropriate condition in later section.

Prior to analyses, the LA-ICP-MS system was calibrated using NIST 613 reference glass for high sensitivity over a large mass range and low production rate of oxides. The production rate of oxide was monitored by ^{248}ThO/^{232}Th and was maintained below 0.5 %. Other potentially interfering oxides were assumed to be negligible compared with the relative ease of Th oxide production (Leichte *et al*., 1987). Basic instrument operating conditions are given in Table 1.

2.2   Standards, analytical elements and data reduction

NIST synthetic silicate glasses of NIST 612-613 and NIST 610-611 were used as external calibration materials in this study. There are sufficient records of these standards as calibration materials for LA-ICP-MS (e.g., Jochum *et al*., 2011), and the concentration of elements in NIST 612-613 is appropriate for analysis of common silicate minerals and glasses (e.g., Mason, *et al*., 1999; Jackson, 2008). In this study, recent values by Jochum *et al*. (2011) along with ISO guidelines were used as reference values for NIST standards, although preferred values of Pearce *et al*. (1997) were adopted for external calibration with NIST 612-613 in most of the previous studies (e.g., Horn *et al*., 1997; Mason *et al*., 1999; Kurosawa *et al*., 2002; Morishita *et al*., 2005).

Analytical elements, mass numbers, and dwell time in this study are shown in Table 2. The dwell time and number of elements are important parameters in optimizing data acquisition procedures (e.g., Günther *et al*., 1999). Measurement of a large number of elements with a long dwell time for each element results in long acquisition times with ICP-MS, which can lead to attenuation of the signal intensity due to the long laser ablation time. For recent LA-ICP-MS analyses, the time-resolved analysis (TRA) mode has been adopted by many institutions (e.g., Longerich *et al*., 1996; Horn *et al*., 1997; Kurosawa *et al*., 2002; Morishita *et al*., 2005). Although an advantage of the TRA mode is a reduction of the signal spike which affect the

analytical precision during unstable sample introduction of the LA system, the spectrum mode makes it easier to understand that counting errors depend on low signal intensity expected with lower concentration samples and/or small laser spot diameter, because the measurement deviation for several sets of replicate analyses are given as RSD of the signal counting and quantitative values. LA-ICP-MS analyses are performed with various purposes and various samples in the GSJ-Lab; therefore, an understanding of the limitation of analytical accuracy for each analysis of an unknown by the assayer is very important. In this study, analytical data were collected using the peak hopping and spectrum mode, and 3 sets of 10 scans (sweeps) for 45 elements from ^{45}Sc to ^{238}U with dwell times shown in Table 2. The acquisition time was *ca.* 40 s and the total analysis time including 12 s of shutter-closed laser stabilization time and laser warm-up time for each analysis was *ca.* 60 s. All signal intensities were corrected with respect to the background signal obtained from measurement of a gas blank for 40 s prior to initiating the calibration standard and unknown measurements. ^{42}Ca was used as an internal standard element and analyzed by pulse-counting mode for all analyses.

Data reduction was conducted using MassHunter Workstation software installed with the Agilent 7700 x. Calibration lines were calculated with the calibration standard and calibration blank as one-point external calibration method, and a series of data reduction, which involved subtraction of the gas blank intensity and calculation of the concentration after normalization using the internal standard element, was performed with the MassHunter software. In addition, selective usage of measured calibration standards and calculation of multi-point calibration lines are also possible with the software. The signal count rate, concentration, and RSDs for each element were reported as standard form. The concentration, signal intensity rate, and type of detectors for each element and each scan could also be confirmed and exported.

3. Results and discussion

3.1 Determination of appropriate operating conditions

To establish precise analysis with LA-ICP-MS, it is important to confirm suitable conditions for the He carrier gas flow rate, repetition rate of the laser and laser energy for efficient and stable introduction of ablated aerosol to the ICP-MS (e.g., Kimura *et al.*, 1996; Hirata and Kon, 2008). Optimized instrumental condition was simply evaluated by the maximal values of signal intensity and its stability in this study. Although we tested individual parameters or settings step by step, these parameters and settings were mutually related to precision of final results. Obviously, following each examination is worth to investigate separately for obtaining "ultimate best" conditions. However

such investigations were beyond the purpose of this paper, thus we determined "practical appropriate" conditions for the purpose of simplest and adequate-quality quantitative analyses in this study. The sample used for examination was NIST 613 synthetic silicate glass reference material, unless otherwise specified. In addition, although ICP-MS was used to measure the mass of various ions, these ions are described as elements in this study to avoid complex description.

3.1.1 Flow rate of He carrier gas

Appropriate flow rates of the He carrier gas were examined for the efficient introduction of ablated aerosol into the ICP-MS. For this purpose, the ICP-MS operating conditions were fixed and the laser energy was set at 50 %, while the flow rates of He carrier gas were varied from 0.2 to 0.8 L min^{-1} with a rate of 0.05 L min^{-1} for laser spot diameters of 100, 80, 60, 40, 20, and 10 μm (fluence 11.5 – 19 J cm^{-2}). As described earlier, Ar nabuliser gas flow rate were fixed as 1 L min^{-1}. It is expected that analyses by various sizes of laser spot diameter would be required in case of analyses of silicate "unknown" minerals. Therefore, general tendency of various laser spot diameter were also tested here. The results are shown in Fig. 1.

The operating conditions of the ICP-MS and laser ablation conditions had not been optimized, so that a relatively large scatter was observed in the < 20 μm spot diameter. Nevertheless, common general features were observed, irrespective of laser spot diameter; the signal count rate of relatively high-mass elements increased with the He carrier gas flow rate, whereas the signal count rate of relatively low-mass elements decreased with an increase in the He carrier gas flow rate. This phenomenon suggests the possible occurrence of mass fractionation from laser ablation to counting in the ICP-MS. Elemental fractionation in LA-ICP-MS has been generally well known in previous studies and several authors have reported different behaviors for different elemental groups, specifically the lithophile, siderophile, and chalcophile elements (e.g., Jackson, 2008). It has been reported that several factors are related to elemental fractionation, such as ionization potentials (Chen, 1999), element melting and boiling points (Outridge *et al.*, 1997), and condensation temperatures (Jackson, 2001). According to Jackson (2001), fractionation occurred, in part, due to two different processes controlled by volatility: (1) differential transport of nanoparticles (condensed vapor) and microparticles (quenched liquid droplets) into which different elements were selectively partitioned on the basis of volatility, and (2) differential volatilization of elements during incomplete volatilization of the microparticles in the ICP (see also Koch *et al.*, 2002, 2004; Kuhn and Günther, 2005). The absolute degree of fractionation that occurs during ablation is highly dependent on numerous factors, including the
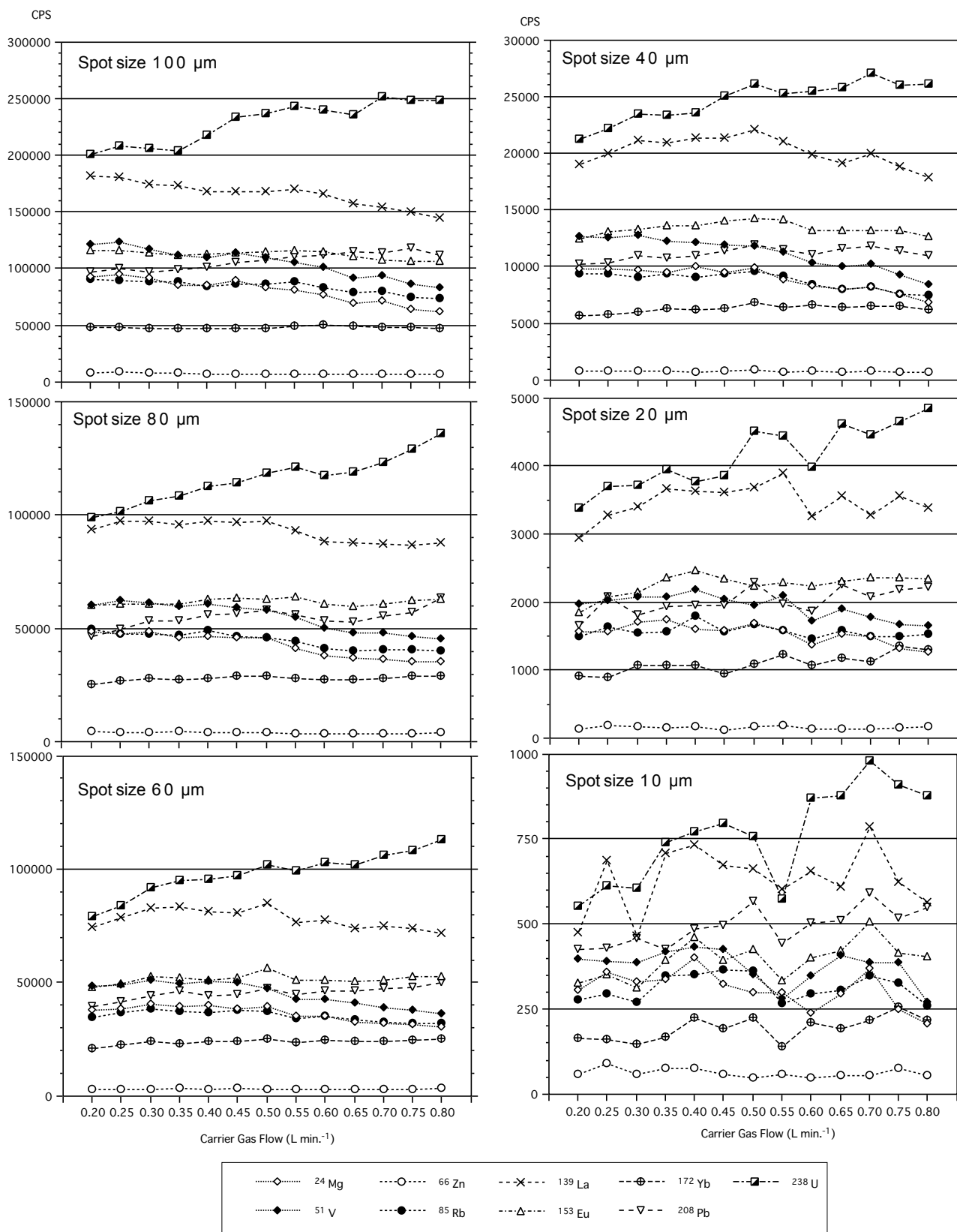
Fig. 1   Relationship between laser spot diameter, He carrier gas flow rate, and signal intensity (count rate). Laser energy and instrumental conditions for ICP-MS were fixed under given conditions, and signal intensities (count per second; CPS) of the NIST 613 reference material with different laser spot sizes and He carrier gas flow rates were measured. See text for detailed discussion.

laser operation conditions (e.g., spot size, pulse energy and/ or pulse width) and the sample matrix (Günther *et al.*, 1999); however, those parameters and the sample were fixed in this study. Although the observed result suggests mass fractionation rather than the elemental fractionation coupled with elemental groups, it is likely that the differential transport of nano- and microparticles with selectively partitioned elements (i.e., light/ heavy elements), and the difference in the ionization position and conditions in the ICP were the primary causes of fractionation. The appropriate conditions for the efficient generation of an aerosol and a relatively optimal He carrier gas flow rate were thus examined.

The most clearest tendency was observed for a 40 μm spot diameter accompanied by correlation between the laser energy and analysis conditions of the ICP-MS. In this case, the signal intensity of ^{153}Eu was almost constant or changed from a slight increase to decrease with an increase in the He carrier gas flow rate. The signal intensities of elements with mass numbers larger than ^{153}Eu were almost constant after increasing the He carrier gas flow rate up to 0.5 L min^{-1}, while that of elements with mass numbers smaller than ^{153}Eu were changed from almost constant up until 0.5 L min^{-1} and were decreased (Fig. 1).

Although the signal intensities varied with different He carrier gas flow rates, the correlation with the signal intensity and concentration between the calibration standard and unknown sample can be ignored when the tendency and rates for variations of correlation between the signal intensities and He carrier gas flow rates were maintained to be constant. Thus, NIST 611 reference materials (450 – 500 μg g^{-1}) were also examined, and similar results that were bordered by a He flow rate if 0.5 L min^{-1} were observed. Based on these results, it is assumed in this study that variation of the signal intensities corresponds to the He carrier gas flow rates and has a constant tendency under appropriate laser ablation conditions, irrespective of the sample concentration and signal intensity itself. Therefore, the boundary of changing tendencies, i.e., 0.5 L min^{-1}, was set as the appropriate flow rate for the He carrier gas.

3.1.2 Laser condition and ablation time

Fig. 2 shows typical spectra with signal intensity (counts per second) versus time at a He carrier gas flow rate of 0.5 L min^{-1}. The time between starting ablation and starting count in the ICP-MS was *ca.* 2.5 s. After a rapid increase of counts, the signal count became a gentle increase for some elements. Therefore, counting was started at 8 s after the laser was switched on in this study. After the end of ablation period, the signal intensity returned to the background level after *ca.* 25 s. The NWR 213 laser system is equipped with an ablation cup just above the ablation point; therefore, the length of time before returning

to the background level was almost constant, regardless of the concentration (signal intensities) of elements in various samples, although the sample chamber is large.

In the LA-ICP-MS method, reference glass materials are generally used as external calibration standard(s) for the measurement of minerals and volcanic glasses. There are differences in the ablation efficiency between the reference glasses and unknown samples (e.g., Eggins *et al.*,1998; Günther and Heinrich,1999). Therefore, internal standardization is necessary for quantitative analysis to compensate these differences of sampling efficiency (e.g., Kimura *et al.*, 2000). ^{29}Si, ^{42}Ca, ^{43}Ca, or ^{44}Ca are commonly used as internal standards, and the concentrations of Si and/or Ca are independently determined using another instrument, such as an electron microprobe analyzer (EPMA). For the method of internal standardization, a quantitative result is obtained from the relationship between the signal intensity ratio of the internal standard element to the target elements, and the concentrations of an external calibration material and measured sample. Therefore, it is not necessary to measure external calibration materials and unknown samples under the same laser conditions; however, suitable measurement conditions for each sample are rather important. For the purpose of microspot analysis, using as small as possible laser spot diameter is frequently required. In such a case, precise measurement of the signal count ratio between the internal standard element and the target elements for external calibration material contribute to improve the accuracy of the quantitative result. Therefore, the laser spot diameter for analysis of the external calibration material was fixed at 100 μm and the appropriate laser conditions were examined.

Sample introduction by laser ablation is relatively unstable compared to that by a nebulizer for the solution method; therefore, considerable variation of the signal intensities is unavoidable. Although an increased repetition rate of the laser pulse led to a more continuous and stable signal, defocusing of the laser and attenuation of the signal intensity due to a higher ablation rate also occurred simultaneously (e.g., Kimura *et al.*, 1996; Hirata and Kon, 2008). Consequently, the integration time could possibly be limited by increasing repetition rate. Thus, optimization of the laser energy, repetition rate, and acquisition time with a suitable carrier gas flow rate is required for stable and precise signal counting. To determine the appropriate laser ablation conditions for an external calibration material, test analyses with change in the laser energy at 5 % steps from 30 – 45 % (fluence 0.2 – 4.0 J cm^{-2}) were conducted at a He carrier gas flow of 0.5 L min^{-1} and with a laser spot diameter of 100 μm. Three sets of 20 scans for 45 elements from ^{45}Sc to ^{238}U were performed using the ICP-MS, and the stability of three replicate analyses was evaluated according to the relative
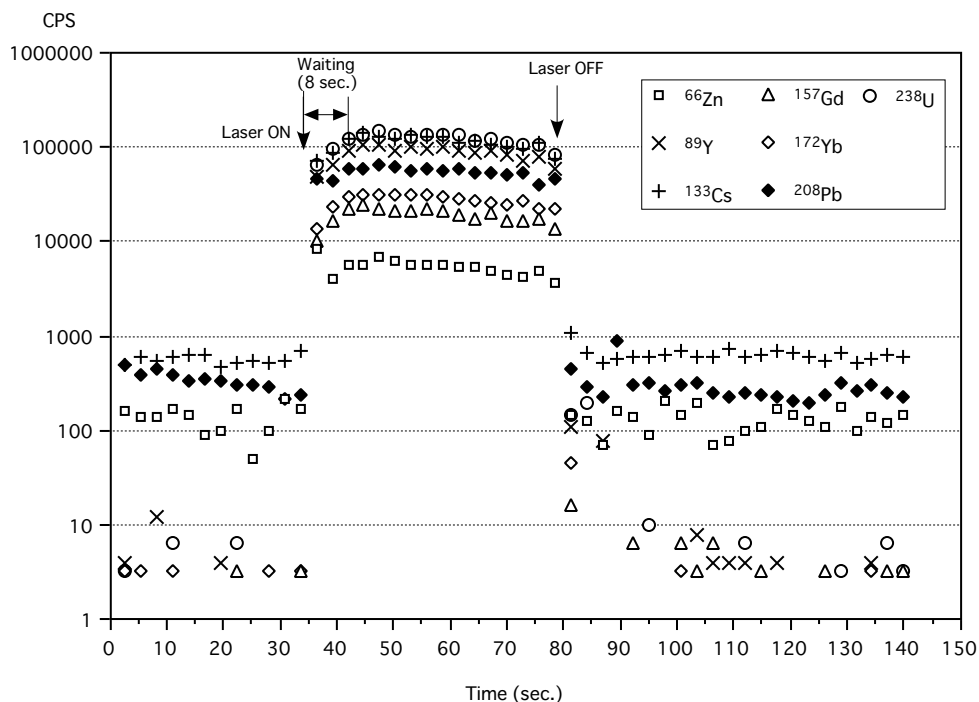
Fig. 2   Typical LA-ICP-MS calibration spectra for ^{66}Zn, ^{89}Y, ^{133}Cs, ^{157}Gd, ^{172}Yb, ^{208}Pb, and ^{238}U showing intensity (CPS) versus time for NIST 613 glass using a 100 μm pit diameter. The acquisition procedure included background measurement of the dry plasma for 40 s prior to ablation for 50 s. After ablation was stopped, the signal returned to background levels after *ca*. 25 s.

standard deviation (RSD) of the signal intensities. The results are shown in Fig. 3.

From a comparison of different laser energies, an RSD of *ca*. 20 % for signal intensities at laser energies of 40 % (fluence *ca*. 2.0 J cm^{-2}) and 45 % (fluence *ca*. 6.0 J cm^{-2}) was the smallest level, and that at 40 % was slightly better than that at 45 % (Fig. 3). In the case of 35 % laser energy, RSD was relatively large (*ca*. 30 %), and that at 30 % laser energy was very large due to insufficient ablation.

A laser energy of 40 % (fluence *ca*. 2.0 J cm^{-2}) at a He carrier gas flow of 0.5 L min^{-1} and a laser spot diameter of 100 μm was thus regarded as the most appropriate condition for ablation of the external calibration material. One of the reasons for the large (20 %) RSD with this condition would be defocusing by ablation. Therefore, the effect of focusing during laser ablation (continuous z-focus) was also examined. The results of laser ablation with continuous z-focus show an RSD of less than 15 % for many elements (Fig. 3); therefore, the analytical precision of for measurement of the external calibration material were improved compared to that without continuous z-focus (fixed z-axis ablation).

According to analytical reports from other institutions, recent analytical protocols adopted by other institutions were laser pulse repetition rates of 5 Hz or 10 Hz (e.g., Eggins and Shelley,

2002; Kurosawa *et al*., 2002; Morishita *et al*., 2005; Regnery *et al*., 2010). Although both 5 Hz and 10 Hz were tested with the same conditions of He carrier gas flow rate and laser energy, there was no advantage for a laser pulse repetition rate of 10 Hz, while adequately stable signal intensities were obtained at 5 Hz, as shown by Fig. 2. Increasing the laser pulse repetition rate results in an increase in the ablation rate at the same laser power. Such aggressive ablation could be a possible cause of mechanical prevention of recovering aerosols by the crater wall, the so-called crater effect (Mason and Mank, 2001). A lower repetition rate contributes to preventing such a phenomenon that is impossible to compensate for solely by the use of continuous z-focus; therefore, of laser pulse repetition rate of 5 Hz was adopted in this study. Analytical conditions of LA system for calibration standard are summarized in Table 1b.

3.2 Analytical results of reference materials
3.2.1 Sensitivity and detection limits

Table 3 shows the analytical results for NIST 615 using NIST 613 as an external calibration standard, typical background count rates, and the lower limit of detection (DL) calculated using sensitivities for each pit diameter. The results for NIST 613 using NIST 611 as an external calibration standard are shown in Table 4. The results for the calibration blank measured before each
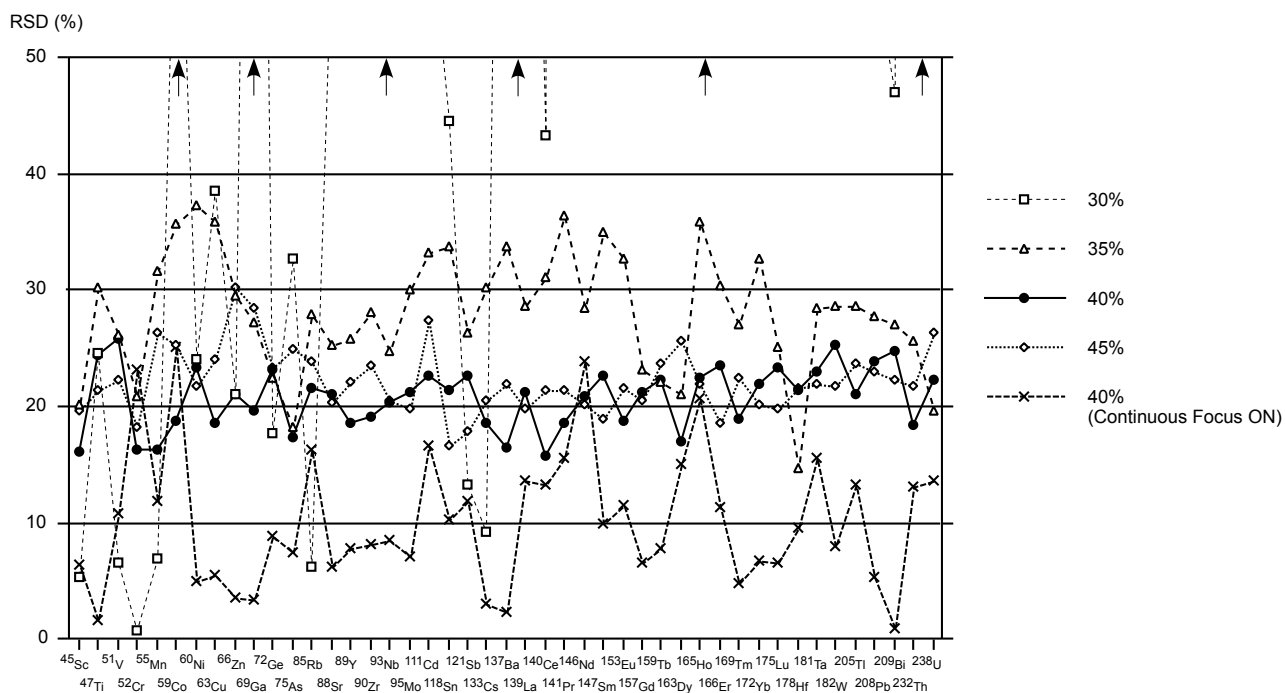
Fig. 3 Relative standard deviations (RSD) of the intensity (CPS) determined for NIST 613 with various laser energy and in continuous z-focus mode.

five replicate analyses are shown as a typical background count because the background drifts during the replicate analyses. The DL and sensitivity were calculated according to the widely used method reported by Longerich *et al*. (1996). Although the DL should be calculated for each element and each analytical result (Longerich *et al*., 1996), for convenience, the averaged values of individual replicate analyses are shown in Table 3 and Table 4. The DL tends to improve with an increase in of the amount of material sampled, as suggested by Morishita *et al*. (2005).

3.2.2 Analytical precision and accuracy

Laser spot diameters of 100, 80, 40, and 20 μm for NIST 615, and 80, 40, 20, and 10 μm for NIST 613 were used for the analyses. Five replicate analyses were performed for each laser spot size and NIST glass. The averaged values, and the DIFs between the averaged and reference values of Jochum *et al*. (2011) (absolute value, DIF; percentage of DIF in reference value, DIF%), and standard deviation (SD) and relative standard deviation (RSD) replicate analyses were also shown in Table 3 and Table 4. Fig. 4 shows DIF % for the reference value reported by Jochum *et al*. (2011).

The numbers of elements in multi-element LA-ICP-MS analysis of geologic samples are generally less than 30 elements, and division into two sets of data acquisition is often adopted for analysis with a large number of elements (> 30 elements)

(e.g., Horn *et al*., 1997; Kurosawa *et al*., 2002; Morishita *et al*., 2005). Therefore, analysis of the 45 elements (+1 internal standard element) in this study covered a very wide range of mass numbers compared to common analytical methods used in many institutions. Nevertheless, the reproducibility (precision) was mostly < 10 % with laser spot diameters of 100 – 80 μm for NIST 615, and only Ni and Zn in 100 μm and Ni in 80 μm were over 15 %. In the case of laser spot diameters < 40 μm, the RSDs were relatively large, and the sensitivity was small for 20 μm. For analyses of NIST 613, the RSDs of the signal intensities were < 10 % for all elements with laser spot diameters > 40 μm and < 15 % for all elements in a 20 – 10 μm laser spot diameter.

For evaluation of accuracy, the analytical results for NIST 615 using NIST 613 as an external calibration standard are shown in Table 3 and Fig. 4a. For laser spot diameters of 100 – 40 μm, all elements except for Sc in all laser spot diameters and Mn at 40 μm, the DIF was less than 30 %. On the other hand, in case of a 20 μm laser spot diameter, the DIFs of 11 elements were over 30 %. Specifically, Ti, V, Mn, Co, Ni, Zn, Ge, Rb, Sr, Y, Zr, Nb, Mo, Cd, Sn, Sb, Cs, Na, La, Ce, Pr, Eu, Gd, Tb, Dy, Ho, Er, Tm, Yb, Lu, Hf, Ta, W, Tl, Pb, Bi, Th, and U for a laser spot diameter of 100 μm, Ti, V, Mn, Co, Ni, Zn, As, Rb, Sr, Y, Nb, Mo, Cd, Sn, Sb, Cs, Ba, La, Ce, Pr, Nd, Sm, Eu, Er, Tm, Yb, Lu, Ta, W, Tl, Pb, Bi, and U for 80 μm, Ti, Ni, Ga, Rb, Sr, Nb, Sn, Sb, Cs, Ba, La, Pr, Eu, Ta, Tl, Pb, Bi, and U for 40 μm, and

Table 3 Quantitative results of replicate analyses (*N=5*) for NIST 615 determined using four pit diameters (100, 80, 40 and 20 μm).

	RV (μg g⁻¹)	BG (cps)	100 μm AV (μg g⁻¹)	DIF (μg g⁻¹)	DIF% (%)	SD (1σ) (μg g⁻¹)	RSD (%)	Sensitivity (cps/μg g⁻¹)	DL (μg g⁻¹)	80 μm AV (μg g⁻¹)	DIF (μg g⁻¹)	DIF% (%)	SD (1σ) (μg g⁻¹)	RSD (%)	Sensitivity (cps/μg g⁻¹)	DL (μg g⁻¹)
Sc	0.74	348	2.46	1.72	232	0.056	2.26	865	0.000	2.26	1.52	205	0.069	3.05	937	0.001
Ti	3.61	21.1	3.46	0.15	4.05	0.340	9.82	51	0.009	3.29	0.32	9.0	0.343	10.4	57	0.016
V	1.01	28.9	1.01	0.00	0.49	0.038	3.74	1077	0.000	1.01	0.00	0.23	0.009	0.9	1143	0.001
Cr	1.19	61.1	1.04	0.15	12.34	0.073	7.0	102	0.006	1.02	0.17	14.18	0.150	14.73	112	0.008
Mn	1.42	1017	1.47	0.05	3.7	0.141	9.55	1152	0.001	1.37	0.05	3.7	0.198	14.5	1312	0.001
Co	0.79	10.67	0.75	0.04	4.92	0.039	5.16	975	0.001	0.74	0.05	6.4	0.038	5.12	1063	0.001
Ni	1.1	158	1.16	0.06	5.6	0.238	20.5	200	0.003	1.09	0.01	1.3	0.170	15.62	209	0.005
Cu	1.37	137	1.82	0.45	33.1	0.085	4.64	485	0.001	1.74	0.37	26.8	0.106	6.11	524	0.002
Zn	2.79	34.7	3.03	0.24	8.48	0.599	19.79	72	0.011	2.71	0.08	2.8	0.395	14.6	79	0.016
Ga	1.31	6.7	1.16	0.15	11.81	0.040	3.47	867	0.001	1.17	0.14	11.00	0.088	7.52	896	0.001
Ge	0.942	133	1.04	0.09	10.0	0.099	9.59	319	0.003	1.04	0.10	10.8	0.135	13.0	314	0.004
As	0.74	8.0	0.65	0.09	12.55	0.078	12.1	102	0.008	0.71	0.03	4.27	0.173	24.5	102	0.011
Rb	0.855	20.0	0.85	0.01	0.98	0.071	8.35	1111	0.000	0.81	0.04	5.12	0.022	2.73	1242	0.001
Sr	45.8	2.67	47.5	1.7	3.63	0.638	1.34	1407	0.000	45.8	0.0	0.04	0.721	1.57	1561	0.001
Y	0.79	2.67	0.79	0.00	0.52	0.041	5.12	1410	0.000	0.85	0.06	7.1	0.057	6.74	1558	0.001
Zr	0.848	0.00	0.93	0.08	9.34	0.051	5.53	714	0.001	0.98	0.13	15.4	0.076	7.72	787	0.001
Nb	0.824	2.67	0.82	0.01	0.61	0.051	6.24	1467	0.000	0.81	0.01	1.70	0.040	4.9	1612	0.001
Mo	0.8	0.00	0.79	0.01	1.14	0.047	5.93	274	0.002	0.80	0.00	0.44	0.047	5.9	299	0.003
Cd	0.56	5.8	0.55	0.01	2.6	0.046	8.4	67	0.013	0.57	0.01	1.11	0.069	12.1	73	0.015
Sn	1.68	58.7	1.59	0.09	5.65	0.094	5.93	506	0.001	1.58	0.10	6.08	0.126	8.0	554	0.002
Sb	0.79	5.3	0.76	0.03	4.25	0.024	3.22	620	0.001	0.72	0.07	8.25	0.063	8.8	667	0.002
Cs	0.664	177	0.71	0.04	6.6	0.042	5.98	1735	0.000	0.70	0.04	6.1	0.093	13.15	1914	0.001
Ba	3.2	0.00	3.46	0.26	7.98	0.126	3.65	228	0.001	3.28	0.08	2.54	0.100	3.05	257	0.004
La	0.72	2.67	0.72	0.00	0.63	0.054	7.61	1777	0.000	0.74	0.02	2.37	0.050	6.8	2005	0.000
Ce	0.813	0.00	0.82	0.01	1.10	0.021	2.51	2022	0.000	0.78	0.04	4.58	0.027	3.4	2241	0.000
Pr	0.768	4.00	0.82	0.06	7.17	0.038	4.57	2187	0.000	0.78	0.01	1.77	0.044	5.67	2517	0.000
Nd	0.752	2.67	0.84	0.09	12.33	0.102	12.06	359	0.001	0.81	0.06	8.05	0.106	13.1	403	0.002
Sm	0.754	0.00	0.83	0.08	10.25	0.071	8.5	297	0.001	0.79	0.03	4.39	0.079	10.0	353	0.003
Eu	0.77	5.33	0.80	0.03	3.44	0.041	5.10	1224	0.000	0.79	0.02	2.12	0.042	5.4	1391	0.001
Gd	0.763	2.22	0.80	0.04	5.41	0.067	8.3	310	0.002	0.84	0.08	10.2	0.083	9.9	354	0.002
Tb	0.739	2.67	0.81	0.07	9.65	0.045	5.52	2008	0.000	0.85	0.11	14.9	0.067	7.86	2316	0.000
Dy	0.746	0.00	0.79	0.05	6.19	0.051	6.42	490	0.001	0.83	0.08	10.7	0.063	7.65	559	0.001
Ho	0.749	2.67	0.78	0.03	3.54	0.019	2.42	1937	0.000	0.84	0.09	11.7	0.033	3.9	2221	0.000
Er	0.74	0.00	0.79	0.05	6.47	0.045	5.76	661	0.001	0.80	0.06	8.04	0.024	3.0	749	0.001
Tm	0.732	2.22	0.74	0.01	1.49	0.043	5.82	2035	0.000	0.78	0.05	6.40	0.027	3.53	2388	0.000
Yb	0.777	1.11	0.77	0.01	0.83	0.016	2.07	450	0.001	0.85	0.07	9.30	0.042	4.93	500	0.001
Lu	0.732	2.22	0.78	0.05	6.19	0.041	5.29	1950	0.000	0.80	0.07	9.5	0.034	4.26	2264	0.000
Hf	0.711	1.11	0.76	0.05	7.43	0.041	5.40	602	0.001	0.83	0.12	16.92	0.087	10.5	668	0.001
Ta	0.808	1.11	0.77	0.03	4.18	0.022	2.86	2225	0.000	0.80	0.01	1.00	0.009	1.07	2506	0.000
W	0.806	2.22	0.80	0.00	0.20	0.040	5.02	609	0.001	0.76	0.05	6.1	0.063	8.30	691	0.001
Tl	0.273	4.4	0.28	0.01	4.21	0.015	5.32	1368	0.000	0.28	0.01	3.57	0.018	6.52	1536	0.001
Pb	2.32	60.0	2.38	0.06	2.79	0.066	2.78	1049	0.000	2.38	0.06	2.60	0.063	2.7	1190	0.001
Bi	0.581	4.4	0.58	0.00	0.57	0.023	4.00	1747	0.000	0.58	0.00	0.27	0.016	2.8	2002	0.001
Th	0.748	1.11	0.79	0.05	6.22	0.047	5.91	1668	0.000	0.83	0.08	10.31	0.031	3.7	1835	0.000
U	0.823	2.22	0.89	0.06	7.88	0.035	3.92	2182	0.000	0.82	0.00	0.43	0.032	4.0	2573	0.000

	RV (μg g⁻¹)	BG (cps)	40 μm AV (μg g⁻¹)	DIF (μg g⁻¹)	DIF% (%)	SD (1σ) (μg g⁻¹)	RSD (%)	Sensitivity (cps/μg g⁻¹)	DL (μg g⁻¹)	20 μm AV (μg g⁻¹)	DIF (μg g⁻¹)	DIF% (%)	SD (1σ) (μg g⁻¹)	RSD (%)	Sensitivity (cps/μg g⁻¹)	DL (μg g⁻¹)
Sc	0.74	348	1.91	1.17	158	0.296	15.53	231	0.002	2.77	2.03	275	0.203	7.3	91	0.008
Ti	3.61	21.1	3.61	0.00	0.1	0.554	15.32	14	0.072	2.86	0.75	20.8	1.032	36.1	6	0.554
V	1.01	28.9	0.77	0.24	24.2	0.074	9.67	281	0.003	1.01	0.00	0.04	0.196	19.4	109	0.004
Cr	1.19	61.1	0.98	0.21	17.3	0.356	36.2	27	0.094	*1.48*	*0.29*	*24*	*0.957*	*64.6*	*16*	*0.352*
Mn	1.42	1017	0.81	0.61	43	0.198	24.57	324	0.005	1.80	0.38	27	0.830	46.18	126	0.022
Co	0.79	10.67	0.69	0.10	12.1	0.118	16.96	253	0.002	0.80	0.01	1.2	0.269	33.71	105	0.006
Ni	1.1	158	1.10	0.00	0	0.224	20.29	51	0.035	*1.24*	*0.14*	*12*	*0.343*	*27.7*	*20*	*0.231*
Cu	1.37	137	1.74	0.37	27.3	0.253	14.48	129	0.005	1.49	0.12	9	0.364	24.4	50	0.026
Zn	2.79	34.7	2.24	0.55	19.6	1.060	47.25	19	0.090	*2.74*	*0.05*	*1.8*	*0.938*	*34.2*	*7*	*0.431*
Ga	1.31	6.7	1.18	0.13	10.0	0.190	16.09	219	0.003	1.32	0.01	1.1	0.148	11.2	88	0.007
Ge	0.942	133	0.81	0.13	14	0.567	69.9	86	0.037	*1.06*	*0.12*	*13*	*0.583*	*54.9*	*35*	*0.168*
As	0.74	8.0	0.66	0.08	11.0	0.194	29.4	25	0.099	*0.71*	*0.03*	*4*	*0.372*	*52.6*	*10*	*0.359*
Rb	0.855	20.0	0.84	0.01	1.4	0.075	8.84	291	0.001	0.90	0.05	5.60	0.101	11.22	111	0.008
Sr	45.8	2.67	43.7	2.1	4.67	2.209	5.06	380	0.001	45.9	0.1	0.1	3.459	7.54	147	0.002
Y	0.79	2.67	0.92	0.13	16.7	0.066	7.16	392	0.002	0.99	0.20	25.77	0.178	17.9	144	0.005
Zr	0.848	0.00	1.01	0.17	19.59	0.110	10.87	205	0.004	1.25	0.40	47.73	0.211	16.9	76	0.015
Nb	0.824	2.67	0.77	0.05	6.62	0.108	14.02	393	0.001	0.89	0.07	8.30	0.135	15.2	144	0.004
Mo	0.8	0.00	0.67	0.13	16.5	0.138	20.7	74	0.012	0.83	0.03	3.5	0.302	36.5	29	0.063
Cd	0.56	5.8	0.46	0.10	17.64	0.177	38.3	17	0.202	0.56	0.00	0.5	0.323	57.4	8	0.536
Sn	1.68	58.7	1.52	0.16	9.76	0.137	9.05	138	0.005	1.97	0.29	17.4	0.491	24.91	52	0.012
Sb	0.79	5.3	0.72	0.07	8.36	0.112	15.47	160	0.006	0.60	0.19	23.56	0.225	37.3	60	0.031
Cs	0.664	177	0.63	0.03	4.4	0.194	30.64	481	0.002	0.63	0.03	4.4	0.324	51.1	192	0.016
Ba	3.2	0.00	3.00	0.20	6.29	0.499	16.64	66	0.006	2.98	0.22	6.9	0.387	13.0	24	0.037
La	0.72	2.67	0.71	0.01	0.78	0.056	7.80	487	0.001	0.76	0.04	6.2	0.089	11.68	182	0.003
Ce	0.813	0.00	0.71	0.10	12.2	0.060	8.43	554	0.001	0.86	0.05	6.2	0.103	11.97	203	0.002
Pr	0.768	4.00	0.73	0.04	5.08	0.063	8.64	634	0.001	0.86	0.09	12.2	0.142	16.4	228	0.003
Nd	0.752	2.67	0.83	0.08	10.75	0.035	4.2	102	0.005	0.72	0.04	4.86	0.107	14.9	40	0.040
Sm	0.754	0.00	0.86	0.11	14.0	0.198	23.0	88	0.008	0.89	0.14	18.05	0.215	24.2	31	0.040
Eu	0.77	5.33	0.80	0.03	4.18	0.089	11.1	350	0.002	0.83	0.06	8.3	0.099	11.91	124	0.006
Gd	0.763	2.22	0.85	0.09	11.52	0.226	26.58	90	0.005	0.98	0.22	28.60	0.170	17.3	31	0.025
Tb	0.739	2.67	0.89	0.15	20.92	0.054	6.02	592	0.001	1.03	0.29	39.80	0.197	19.07	211	0.003
Dy	0.746	0.00	0.89	0.14	19.34	0.100	11.2	145	0.003	0.87	0.12	16.4	0.069	8.0	50	0.021
Ho	0.749	2.67	0.89	0.15	19.43	0.087	9.7	570	0.001	1.03	0.28	37.27	0.196	19.06	197	0.003
Er	0.74	0.00	0.88	0.14	18.81	0.093	10.6	193	0.003	0.93	0.19	26.31	0.123	13.2	67	0.012
Tm	0.732	2.22	0.87	0.14	18.66	0.065	7.46	615	0.001	0.92	0.18	25.06	0.033	3.6	207	0.003
Yb	0.777	1.11	0.89	0.11	14.5	0.148	16.6	132	0.004	0.92	0.14	18.25	0.235	25.6	44	0.021
Lu	0.732	2.22	0.86	0.13	18.03	0.039	4.52	602	0.001	0.97	0.24	32.24	0.101	10.46	196	0.002
Hf	0.711	1.11	0.85	0.14	19.72	0.127	14.9	179	0.005	0.89	0.17	24.61	0.197	22.3	60	0.020
Ta	0.808	1.11	0.81	0.00	0.32	0.070	8.59	636	0.001	0.96	0.16	19.28	0.083	8.59	216	0.002
W	0.806	2.22	0.71	0.09	11.7	0.098	13.8	163	0.004	0.81	0.01	0.9	0.135	16.6	61	0.012
Tl	0.273	4.4	0.26	0.02	6.29	0.045	17.6	379	0.002	0.27	0.01	1.25	0.076	28.3	127	0.011
Pb	2.32	60.0	2.34	0.02	0.74	0.209	8.96	291	0.001	2.65	0.33	14.1	0.298	11.24	99	0.005
Bi	0.581	4.4	0.56	0.02	3.5	0.063	11.19	496	0.001	0.59	0.01	1.0	0.043	7.3	171	0.004
Th	0.748	1.11	0.87	0.13	16.81	0.062	7.11	480	0.001	0.95	0.21	27.48	0.089	9.4	176	0.003
U	0.823	2.22	0.76	0.06	7.2	0.069	9.04	650	0.001	0.82	0.00	0.5	0.100	12.22	227	0.002

RV: reference value of Jochum *et al.* (2011), AV: averaged value of analytical result, DIF: difference from reference value, DIF%: percentage of DIF against RV, SD: standard deviation of analytical values, RSD: relative standard deviation of analytical values, LD: lower limit of detection.

*Values shown by *Italic* are reference values. Because of low background−signal count ratio, results of those elements were not determined in several sets, thus those values were extrapolated from other sets of analyses (*N=5*).

Table 4 Quantitative results of replicate analyses (*N=5*) for NIST 613 determined using four pit diameters (80, 40, 20 and 10 μm).

	RV ($\mu g\,g^{-1}$)	BG (cps)	80 μm							40 μm						
			AV ($\mu g\,g^{-1}$)	DIF ($\mu g\,g^{-1}$)	DIF% (%)	SD (1σ) ($\mu g\,g^{-1}$)	RSD (%)	Sensitivity (cps/$\mu g\,g^{-1}$)	DL ($\mu g\,g^{-1}$)	AV ($\mu g\,g^{-1}$)	DIF ($\mu g\,g^{-1}$)	DIF% (%)	SD (1σ) ($\mu g\,g^{-1}$)	RSD (%)	Sensitivity (cps/$\mu g\,g^{-1}$)	DL ($\mu g\,g^{-1}$)
Sc	39.9	227	34.5	5.4	13.54	1.29	3.75	1000	0.001	36.7	3.2	8.12	0.85	2.31	251	0.001
Ti	44	11.1	38.0	6.0	13.6	1.89	4.97	57	0.021	36.7	7.3	16.5	2.73	7.44	14	0.025
V	38.8	22.2	38.8	0.0	0.08	1.86	4.81	986	0.001	38.2	0.6	1.56	0.97	2.54	232	0.001
Cr	36.4	47.8	38.7	2.3	6.37	2.41	6.21	94	0.014	34.7	1.7	4.71	2.20	6.33	24	0.017
Mn	38.7	1103	42.1	3.4	8.86	3.01	7.14	1040	0.001	36.9	1.8	4.66	1.30	3.53	272	0.001
Co	35.5	10.7	35.1	0.4	1.01	1.36	3.88	893	0.001	35.1	0.4	1.15	1.06	3.03	211	0.001
Ni	38.8	141	39.3	0.5	1.34	1.71	4.35	171	0.007	39.5	0.7	1.68	0.92	2.32	42	0.008
Cu	37.8	113	37.9	0.1	0.29	1.07	2.83	430	0.003	39.6	1.8	4.69	0.66	1.66	104	0.002
Zn	39.1	33.3	38.5	0.6	1.6	1.33	3.46	64	0.021	40.3	1.2	2.96	2.34	5.80	15	0.026
Ga	36.9	4.0	38.1	1.2	3.18	1.19	3.12	781	0.002	39.4	2.5	6.83	1.04	2.64	182	0.001
Ge	36.1	247	40.7	4.6	12.7	2.52	6.20	248	0.006	41.7	5.6	15.6	1.60	3.84	59	0.006
As	35.7	14.7	35.7	0.0	0.05	1.85	5.19	86	0.016	36.9	1.2	3.50	2.93	7.92	20	0.016
Rb	31.4	76	31.9	0.5	1.55	1.01	3.17	1025	0.001	32.0	0.6	1.82	0.60	1.88	242	0.001
Sr	78.4	1.3	71.4	7.0	8.89	1.94	2.72	1483	0.001	77.3	1.1	1.35	1.77	2.29	334	0.001
Y	38.3	2.7	32.8	5.5	14.3	1.47	4.47	1772	0.001	37.0	1.3	3.43	1.01	2.72	428	0.001
Zr	37.9	4.0	33.2	4.7	12.3	1.06	3.19	907	0.001	34.4	3.5	9.24	0.75	2.17	236	0.001
Nb	38.9	0.0	37.0	1.9	4.8	1.81	4.88	1496	0.001	35.4	3.5	9.0	0.86	2.43	385	0.001
Mo	37.4	0.0	36.7	0.7	2.00	1.95	5.33	266	0.005	37.0	0.4	0.96	0.68	1.83	62	0.003
Cd	28.1	2.5	29.2	1.1	3.78	1.28	4.38	63	0.019	30.6	2.5	8.78	1.81	5.93	14	0.018
Sn	38.6	33.3	37.7	0.9	2.29	1.66	4.40	510	0.002	39.5	0.9	2.39	1.92	4.86	120	0.002
Sb	34.7	8.0	34.7	0.0	0.14	1.53	4.40	600	0.002	36.1	1.4	4.16	1.54	4.27	138	0.001
Cs	42.7	203	41.4	1.3	3.08	1.30	3.14	1830	0.001	41.0	1.7	3.91	0.70	1.69	426	0.001
Ba	39.3	0.0	38.6	0.7	1.89	1.58	4.11	238	0.005	38.9	0.4	1.0	2.16	5.54	54	0.005
La	36	2.7	34.0	2.0	5.65	1.55	4.56	2007	0.001	35.0	1.0	2.82	0.97	2.78	489	0.001
Ce	38.4	1.3	38.3	0.1	0.18	1.98	5.15	2068	0.001	37.9	0.5	1.25	0.74	1.95	474	0.001
Pr	37.9	1.3	37.7	0.2	0.63	1.93	5.12	2349	0.000	37.9	0.0	0.1	1.23	3.25	566	0.001
Nd	35.5	0.0	33.9	1.6	4.41	0.95	2.80	421	0.002	34.6	0.9	2.46	1.58	4.55	99	0.005
Sm	37.7	0.0	34.3	3.4	9.15	2.00	5.83	377	0.003	40.1	2.4	6.25	1.45	3.63	81	0.004
Eu	35.6	0.0	33.4	2.2	6.17	1.79	5.36	1408	0.001	38.1	2.5	6.97	0.99	2.59	300	0.001
Gd	37.3	4.4	33.0	4.3	11.48	1.42	4.31	416	0.002	38.8	1.5	4.15	1.84	4.73	92	0.004
Tb	37.6	1.3	32.7	4.9	13.00	1.55	4.72	2766	0.000	36.1	1.5	4.07	1.64	4.56	663	0.000
Dy	35.5	0.8	30.7	4.8	13.6	1.63	5.32	679	0.001	35.2	0.3	0.98	1.43	4.07	158	0.002
Ho	38.3	2.7	33.5	4.8	12.6	1.73	5.16	2601	0.000	39.7	1.4	3.69	0.94	2.37	599	0.001
Er	38	1.7	32.8	5.2	13.58	1.63	4.95	896	0.001	39.6	1.6	4.33	1.14	2.87	204	0.001
Tm	36.8	2.2	31.6	5.2	14.20	1.42	4.49	2855	0.000	38.5	1.7	4.56	1.43	3.71	639	0.000
Yb	39.2	1.1	32.4	6.8	17.3	1.18	3.65	634	0.001	39.6	0.4	0.91	1.73	4.38	140	0.002
Lu	37	2.2	34.1	2.9	7.9	0.74	2.18	2621	0.000	35.7	1.3	3.51	1.13	3.16	673	0.000
Hf	36.7	4.4	33.7	3.0	8.16	1.45	4.31	795	0.001	37.8	1.1	3.08	1.08	2.87	193	0.002
Ta	37.6	0.0	33.6	4.0	10.51	1.32	3.92	2687	0.000	38.2	0.6	1.65	1.07	2.81	635	0.000
W	38	2.2	37.6	0.4	1.12	1.86	4.95	604	0.002	42.8	4.8	12.69	1.32	3.09	130	0.001
Tl	14.9	3.3	15.9	1.0	6.4	0.65	4.10	1496	0.001	17.2	2.3	15.25	0.87	5.07	313	0.000
Pb	38.57	28.9	40.0	1.4	3.75	1.04	2.60	1061	0.001	42.7	4.1	10.71	1.40	3.27	231	0.001
Bi	30.2	3.3	36.4	6.2	20.6	0.93	2.55	1541	0.001	36.8	6.6	21.7	1.04	2.83	350	0.000
Th	37.79	2.2	32.9	4.8	12.83	1.42	4.30	2249	0.000	37.7	0.1	0.15	0.74	1.96	503	0.000
U	37.38	8.9	36.0	1.3	3.61	1.06	2.95	2466	0.001	36.5	0.9	2.49	0.73	2.01	539	0.001

	RV ($\mu g\,g^{-1}$)	BG (cps)	20 μm							10 μm						
			AV ($\mu g\,g^{-1}$)	DIF ($\mu g\,g^{-1}$)	DIF% (%)	SD (1σ) ($\mu g\,g^{-1}$)	RSD (%)	Sensitivity (cps/$\mu g\,g^{-1}$)	DL ($\mu g\,g^{-1}$)	AV ($\mu g\,g^{-1}$)	DIF ($\mu g\,g^{-1}$)	DIF% (%)	SD (1σ) ($\mu g\,g^{-1}$)	RSD (%)	Sensitivity (cps/$\mu g\,g^{-1}$)	DL ($\mu g\,g^{-1}$)
Sc	39.9	227	38.1	1.8	4.6	1.24	3.25	114	0.003	39.7	0.2	0.5	2.35	5.91	59	0.004
Ti	44	11.1	42.6	1.4	3.1	1.72	4.0	6	0.082	40.1	3.9	9.0	4.38	10.9	3	0.180
V	38.8	22.2	42.7	3.9	10.2	1.67	3.90	101	0.001	41.3	2.5	6.6	2.10	5.08	59	0.005
Cr	36.4	47.8	36.7	0.3	0.77	2.18	5.95	11	0.034	39.2	2.8	7.6	1.45	3.70	6	0.078
Mn	38.7	1103	36.6	2.1	5.6	1.84	5.04	132	0.002	39.8	1.1	2.8	4.60	11.57	70	0.003
Co	35.5	10.7	35.5	0.0	0.11	0.93	2.62	99	0.002	37.0	1.5	4.1	1.22	3.31	55	0.005
Ni	38.8	141	43.8	5.0	12.77	2.17	4.96	19	0.018	40.8	2.0	5.1	2.37	5.81	11	0.048
Cu	37.8	113	39.9	2.1	5.53	1.32	3.30	48	0.005	41.6	3.8	10.15	1.69	4.05	28	0.008
Zn	39.1	33.3	37.2	1.9	4.9	2.02	5.4	7	0.063	32.7	6.4	16.3	4.57	13.95	4	0.133
Ga	36.9	4.0	38.9	2.0	5.29	1.50	3.86	89	0.002	41.0	4.1	11.0	2.23	5.43	48	0.004
Ge	36.1	247	41.0	4.9	13.6	3.21	7.82	27	0.013	39.9	3.8	10.4	5.32	13.33	15	0.033
As	35.7	14.7	34.3	1.4	4.03	3.47	10.1	10	0.035	37.2	1.5	4.3	4.67	12.55	5	0.114
Rb	31.4	76	32.8	1.4	4.37	0.58	1.76	114	0.001	36.8	5.4	17.25	1.72	4.67	59	0.003
Sr	78.4	1.3	76.9	1.5	1.9	1.88	2.45	156	0.002	76.9	1.5	1.9	4.09	5.32	84	0.004
Y	38.3	2.7	39.4	1.1	2.7	1.12	2.83	189	0.001	37.4	0.9	2.3	1.05	2.81	106	0.003
Zr	37.9	4.0	40.3	2.4	6.3	1.12	2.78	97	0.004	38.1	0.2	0.5	1.94	5.09	55	0.006
Nb	38.9	0.0	38.9	0.0	0.0	1.80	4.62	173	0.001	41.1	2.2	5.7	1.08	2.63	91	0.002
Mo	37.4	0.0	38.4	1.0	2.7	1.47	3.83	30	0.006	43.6	6.2	16.5	2.73	6.26	15	0.014
Cd	28.1	2.5	27.1	1.0	3.6	1.82	6.7	7	0.045	28.8	0.7	2.4	6.17	21.4	3	0.147
Sn	38.6	33.3	41.1	2.5	6.50	1.87	4.56	55	0.003	43.5	4.9	12.6	1.44	3.31	28	0.010
Sb	34.7	8.0	39.1	4.4	12.7	2.66	6.81	60	0.004	39.1	4.4	12.6	2.31	5.91	34	0.006
Cs	42.7	203	49.0	6.3	14.84	1.89	3.86	176	0.001	47.9	5.2	12.27	3.09	6.44	102	0.002
Ba	39.3	0.0	40.2	0.9	2.2	0.60	1.49	25	0.016	39.8	0.5	1.2	2.62	6.59	14	0.025
La	36	2.7	34.4	1.6	4.6	1.29	3.75	234	0.001	37.2	1.2	3.5	1.65	4.44	118	0.002
Ce	38.4	1.3	37.4	1.0	2.7	0.62	1.66	229	0.001	39.2	0.8	2.2	1.65	4.20	119	0.002
Pr	37.9	1.3	33.8	4.1	10.8	1.10	3.25	293	0.001	38.0	0.1	0.2	2.15	5.65	144	0.002
Nd	35.5	0.0	32.3	3.2	8.9	1.75	5.40	50	0.007	35.2	0.3	0.9	1.29	3.65	26	0.013
Sm	37.7	0.0	35.0	2.7	7.0	1.42	4.04	44	0.007	39.3	1.6	4.2	3.47	8.83	22	0.021
Eu	35.6	0.0	32.6	3.0	8.4	0.68	2.10	160	0.001	35.1	0.5	1.4	1.41	4.01	81	0.005
Gd	37.3	4.4	35.8	1.5	4.0	0.47	1.31	47	0.008	35.2	2.1	5.8	1.87	5.31	25	0.018
Tb	37.6	1.3	36.0	1.6	4.4	1.18	3.29	312	0.001	35.7	1.9	5.0	0.77	2.17	168	0.002
Dy	35.5	0.8	34.0	1.5	4.2	0.68	2.00	74	0.003	35.2	0.3	0.9	1.31	3.71	39	0.008
Ho	38.3	2.7	34.7	3.6	9.31	0.88	2.53	308	0.001	36.2	2.1	5.6	2.44	6.75	160	0.002
Er	38	1.7	36.4	1.6	4.3	0.77	2.12	102	0.002	38.0	0.0	0.0	1.83	4.83	51	0.008
Tm	36.8	2.2	36.7	0.1	0.2	1.18	3.21	306	0.001	36.2	0.6	1.6	1.34	3.71	163	0.002
Yb	39.2	1.1	38.4	0.8	2.0	2.00	5.19	67	0.005	35.8	3.4	8.6	3.26	9.11	36	0.009
Lu	37	2.2	35.3	1.7	4.5	1.28	3.62	314	0.001	33.6	3.4	9.2	1.14	3.41	173	0.002
Hf	36.7	4.4	34.6	2.1	5.7	1.13	3.27	96	0.002	37.2	0.5	1.5	2.98	8.01	50	0.007
Ta	37.6	0.0	34.0	3.6	9.5	1.00	2.95	332	0.001	39.0	1.4	3.7	1.71	4.39	163	0.001
W	38	2.2	41.2	3.2	8.5	1.39	3.37	66	0.004	45.3	7.3	19.26	1.82	4.01	34	0.005
Tl	14.9	3.3	17.3	2.4	15.8	0.89	5.2	152	0.001	16.8	1.9	12.7	0.43	2.6	82	0.004
Pb	38.57	28.9	42.9	4.4	11.3	1.68	3.92	106	0.002	43.2	4.6	11.9	1.79	4.14	56	0.003
Bi	30.2	3.3	36.2	6.0	19.87	0.54	1.50	166	0.001	36.9	6.7	22.3	1.27	3.43	86	0.003
Th	37.79	2.2	37.7	0.1	0.2	1.59	4.22	240	0.001	39.2	1.4	3.8	1.28	3.27	129	0.002
U	37.38	8.9	37.0	0.4	1.0	0.77	2.09	249	0.001	41.1	3.7	10.0	1.57	3.81	130	0.002

RV: reference value of Jochum *et al.* (2011), AV: averaged value of analytical result, DIF: difference from reference value, DIF%: percentage of DIF against RV, SD: standard deviation of analytical values, RSD: relative standard deviation of analytical values, LD: lower limits of detection.
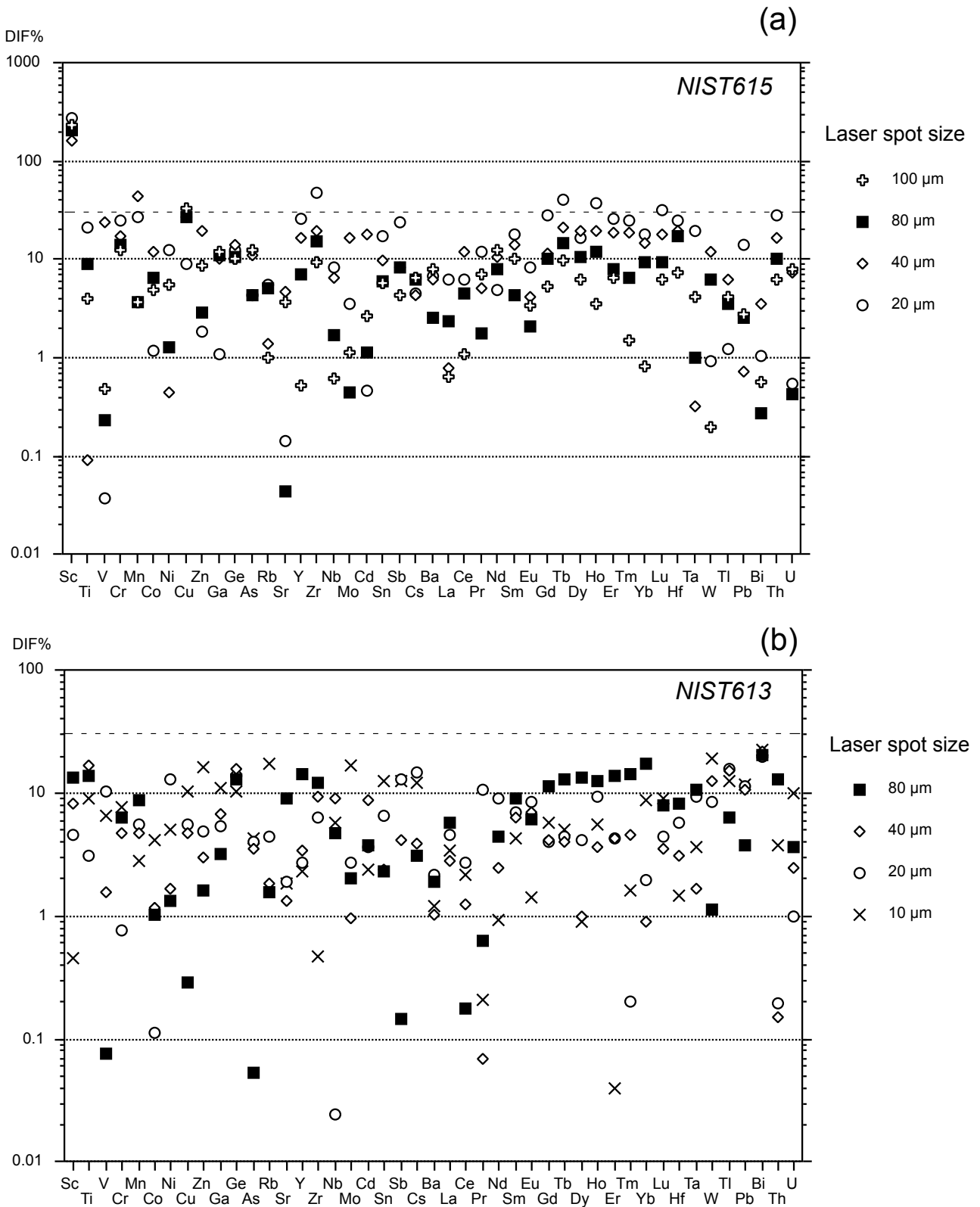
Fig. 4   DIF% for the Ca-normalized values determined for various pit diameters from the reference values by Jochum *et al.* (2011). Values for (a) NIST 615 and (b) NIST 613.

V, Co, Cu, Ga, Rb, Sr, Nb, Mo, Cd, Cs, Ba, La, Ce, Nd, Eu, W, Tl, Bi, and U for 20 μm had DIFs less than 10 %. In addition, As, Nd, and Sm for 100 μm, Cr, Ga, Ge, Gd, Tb, Dy, Ho, and Th for 80 μm, Co, Ge, As, Ce, Nd, Sm, Gd, Yb, and W for 40 μm, and Pr and Pb for 20 μm had DIF < 15 %, while Cr for 100 μm, Cu, Zr, and Hf for 80 μm, V, Cr, Cu, Zn, Y, Zr, Mo, Cd, Tb, Dy, Ho, Er, Tm, Lu, Hf, and Th for 40 μm, and Ti, Mn, Y, Sn, Sb, Sm, Gd, Dy, Er, Tm, Yb, Hf, Ta, and Th for 20 μm had DIFs less than 30 %.

The only elements with poor accuracy for all laser spot diameters was Sc. Relatively high concentration compared to a reference value has also been reported by Kurosawa *et al*. (2002) and Morishita *et al*. (2005). Regnery *et al*. (2010) suggested that molecules at mass number 45 have a strong influence on the accuracy of Sc measurements, especially for Sc < 30 μg g^{-1} when using low mass resolution instruments (quadrupole ICP-MS). As described below, the analytical results for NIST 613 (Sc 39.9 μg g^{-1}) were very precise, and the result supported the suggestion given by Regnery *et al*. (2010). Thus, careful evaluation would be required for accuracy in the quantitative result of Sc < 30 μg g^{-1}. For other elements with poor accuracy, the accuracy was improved, in some cases, even though the laser spot diameter was smaller. The results in these cases suggest that the relatively poor reproducibility affected the accuracy, such as abrupt signal spikes in some replicate analyses. Similarly, for a laser spot diameter of 20 μm, a small signal/background ratio would be the fundamental cause of poor accuracy.

Table 4 and Fig. 4b show the analytical results for NIST 613 using NIST 611 as an external calibration standard. Precision was less than 30 % for all elements and all laser spot sizes. The accuracy was mostly less than 15 % for all laser spot diameters, except for a rather systematically large DIF for Bi. From these results, samples with concentrations similar to that of the NIST 613 reference glass (> 30 μg g^{-1}) can be quantitatively analyzed with accuracy, even with a laser spot diameter of 10 μm with which the precision is small.

Five replicate analyses for NIST 615 and NIST 613 were conducted continuously after the first set of calibration blank and calibration standard analyses. The effect of serious instrumental drift during the five replicate analyses was not observed, as shown in Table 3. Therefore, five replicate analyses after a set of calibration blank and calibration standard analyses was allowed for unknown quantitative analysis.

3.2.3 Crater depths
Penetration of object minerals/glasses during analysis of thin section samples is a potential serious problem during analysis where a large number of elements are measured with a long ablation time. To evaluate the depth of the laser pit (crater) for

analyses of natural clinopyroxene (Cpx), amphiboles (Amp), and plagioclase (Pl), the crater depth was measured under given conditions using a confocal microscopy (HD-100, Lasertec Corporation; 50 × objective lens and numerical aperture 0.95) at the National Metrology Institute of Japan, AIST (Fig. 5). Based on these results, the estimated crater depth for appropriate ablation conditions were determined to be Cpx 26 μm, Amp 19 μm, and Pl 19 μm for a 100 μm laser spot diameter, Cpx 28 μm, Amp 20 μm, and Pl 20 μm for a 40 μm laser spot diameter, and Cpx 28 μm, Amp 18 μm, and Pl 19 μm for a 20 μm laser spot diameter. Although analysis of Cpx requires care, penetration would not occur for thin section samples with a standard thickness of *ca*. 30 μm.

4. Application: analytical condition and accuracy for analyses of silicate minerals

In the previous sections, analysis of 45 elements (+ 1 internal standard element) in a single run was discussed. The analysis of such a large number of elements with a single run is not common, and a reduction of the analyte elements and ablation time, and/or an increase in the number of sweep times appropriate for the analytical objective would lead to more stable and accurate results. Although it is presumed that an analytical protocol and its accuracy for a particular geochemical object would be reported separately, two suites of analytical programs for the general discussion of petrological and geochemical studies on silicate minerals and volcanic glasses were prepared in this study. The precision and accuracy of those two sets are reported below as general-purpose analytical programs in the GSJ-Lab.

4.1 Set 1 (Sc, Ti, V, Mn, Co, Ni, Cr, Rb, Sr, Y, Zn, Zr, Nb, Cs, Ba, lanthanides, Hf, Ta, Pb, Th and U)
As assumed analytical objects of Cpx, Amp, garnet, and biotite, an analytical program for 34 elements (+ 1 internal standard element) of Sc, Ti, V, Mn, Co, Ni, Cr, Rb, Sr, Y, Zn, Zr, Nb, Cs, Ba, lanthanides, Hf, Ta, Pb, Th, and U was prepared as Set 1. In Set 1, the sweep of the entire mass range was increased to 30 times, owing to a reduction of acquisition time for a single scan. As a result, the total acquisition time was *ca*. 34 s. Using the Set 1 program, five times replicate analyses with laser spot diameters of 80, 40, 20, and 10 μm were conducted on NIST 615 using NIST 613 as an external calibration standard. The averaged results, DIFs between the averaged and reference values by Jochum *et al*. (2011), SD, RSD, sensitivity, and DL are given in Table 5.

Precision was mostly less than 20 % for 80 – 40 μm laser spot diameters and less than 30 % for a 20 μm laser spot diameter, although many of the elements were > 30 % for a 10 μm laser
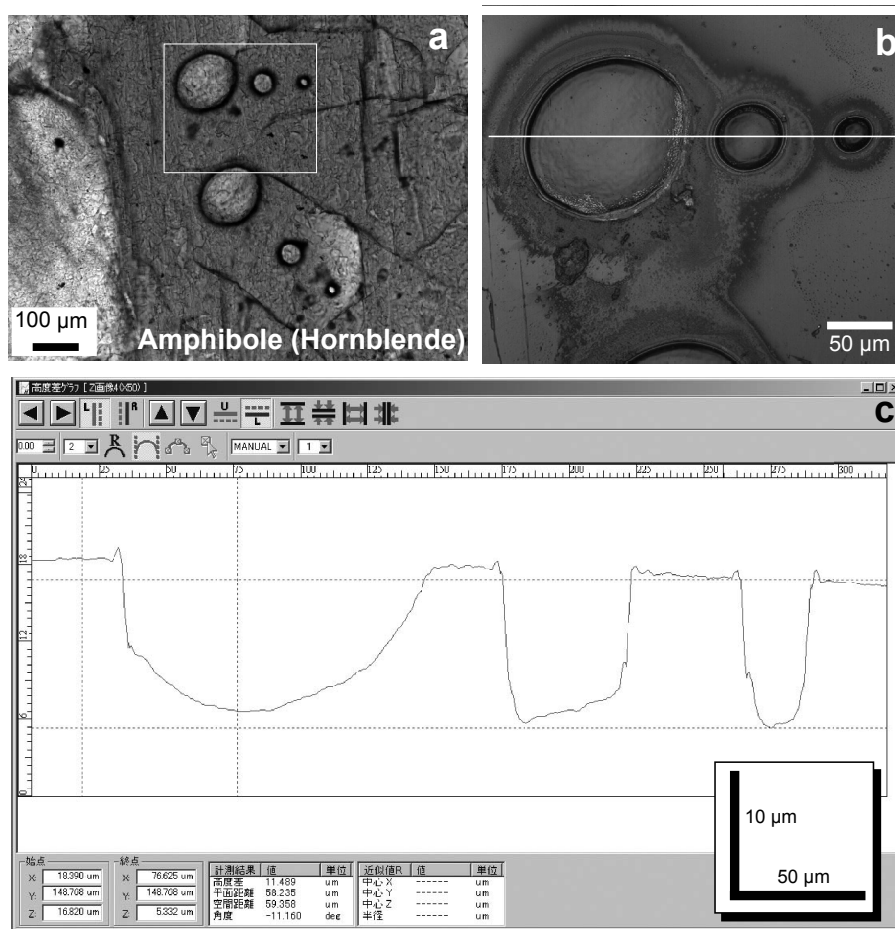
Fig. 5　Example of crater depth measurement using a confocal microscope. (a) Photomicrograph of crater after laser ablation of hornblende (open Nicol). The square indicates the location of panel (b). (b) All-focused confocal microscope image. The image area was scanned by many slices of focuses and reconstructed as an all-focus image. The white line across the center of the crater indicates the location of panel (c). (c) Software screen showing surface profile along the line in panel (b). Precise measurement on any two points is possible. Note: scale bar is superimposed on the screenshot for convenience.

spot diameter. A comparison of the analytical results and reference values by Jochum *et al*. (2011) is shown in Fig. 6. DIFs for all elements and for all laser spot sizes were less than 30 %, except for Sc. For spot sizes of 20 and 10 μm, quantitative results could not be obtained for some elements in some runs because the background intensities were larger than the signal intensities. While quantitative values were obtained, the values were not far from those by Jochum *et al*. (2011); therefore, these results are shown as the reference values in this study.

The estimated crater depths for analyses of Cpx, Amp, and Pl using the Set 1 program were Cpx 23 μm, Amp 17 μm, and Pl 16 μm for a laser spot diameter of 100 μm, Cpx 24 μm, Amp 17 μm, and Pl 17 μm for a 40 μm diameter, and Cpx 25 μm, Amp 16 μm, and Pl 17 μm for a 20 μm diameter. Thus, penetration would not occur during analyses of standard thickness thin section samples (*ca*. 30 μm).

4.2　Set 2 (Sc, V, Rb, Sr, Y, Zr, Nb, Ba, lanthanides, Hf, Ta, Pb, Th and U)

As assumed analytical objects of Pl, an analytical program for 27 elements (+ 1 internal standard element) of Sc, V, Rb, Sr, Y, Zr, Nb, Ba, lanthanides, Hf, Ta, Pb, Th, and U was prepared as Set 2. Sweeps were increased to 50 times for Set 2 and the total acquisition time was *ca*. 32 s. Using the Set 2 program, five times replicate analyses for laser spot diameters of 80, 40, 20, and 10 μm were conducted on NIST 615 using NIST 613 as an external calibration standard. Averaged results, DIFs between the averaged and reference values by Jochum *et al*. (2011), SD, RSD, sensitivity, and DL are given in Table 6.

Precision was less than 20 % for all elements for 80 – 40 μm laser spot diameters. For laser spot sizes of 20 and 10 μm, several elements showed precision greater than 30 %. A comparison of the analytical results and reference values by Jochum *et al*.

Table 5   Quantitative results of replicate analyses (*N*=5) for NIST 615 determined using four pit diameters (80, 40, 20, and 10 μm) by elemental Set 1.

	RV (μg g⁻¹)	80 μm AV (μg g⁻¹)	DIF (μg g⁻¹)	DIF% (%)	SD (1σ) (μg g⁻¹)	RSD (%)	Sensitivity (cps/μg g⁻¹)	DL (μg g⁻¹)	40 μm AV (μg g⁻¹)	DIF (μg g⁻¹)	DIF% (%)	SD (1σ) (μg g⁻¹)	RSD (%)	Sensitivity (cps/μg g⁻¹)	DL (μg g⁻¹)
Sc	0.74	2.95	2.21	298	0.190	6.44	1292	0.001	3.36	2.62	354	0.452	13.44	293	0.001
Ti	3.61	2.84	0.77	21.4	0.436	15.4	77	0.013	3.54	0.07	2.02	1.216	34.4	15	0.087
V	1.01	0.93	0.08	8.39	0.082	8.89	1499	0.001	1.06	0.05	5.42	0.161	15.08	292	0.002
Cr	1.19	0.89	0.30	25.59	0.163	18.5	144	0.007	1.05	0.14	11.7	0.718	68.4	30	0.068
Mn	1.42	1.33	0.09	6.2	0.096	7.23	1655	0.001	1.39	0.03	2	0.566	40.81	324	0.005
Co	0.79	0.71	0.08	10.7	0.021	2.94	1292	0.001	0.86	0.07	8.5	0.097	11.37	278	0.002
Ni	1.1	0.87	0.23	21.2	0.108	12.43	268	0.004	0.97	0.13	12.2	0.459	47.5	58	0.046
Zn	2.79	2.47	0.32	11.6	0.283	11.48	91	0.012	3.36	0.57	20.4	0.796	23.7	20	0.085
Rb	0.855	0.90	0.05	5.53	0.077	8.58	1352	0.001	0.91	0.05	6.3	0.027	2.92	259	0.002
Sr	45.8	43.7	2.1	4.48	1.946	4.45	1736	0.000	47.1	1.3	2.83	1.569	3.33	335	0.000
Y	0.79	0.81	0.02	3.10	0.037	4.51	1705	0.000	0.82	0.03	3.2	0.082	10.10	398	0.001
Zr	0.848	0.85	0.00	0.00	0.088	10.38	929	0.001	0.99	0.15	17.3	0.076	7.66	215	0.002
Nb	0.824	0.82	0.00	0.23	0.007	0.81	1782	0.000	0.84	0.02	2.53	0.046	5.4	385	0.001
Cs	0.664	0.76	0.09	13.9	0.144	19.0	1987	0.000	0.77	0.11	16.5	0.067	8.62	401	0.001
Ba	3.2	3.08	0.12	3.78	0.170	5.51	259	0.004	3.21	0.01	0.32	0.327	10.20	51	0.008
La	0.72	0.70	0.02	3.33	0.011	1.56	1999	0.000	0.76	0.04	5.57	0.086	11.32	447	0.001
Ce	0.813	0.75	0.06	7.5	0.055	7.31	2253	0.000	0.84	0.03	3.35	0.088	10.46	465	0.001
Pr	0.768	0.73	0.04	4.68	0.032	4.34	2508	0.000	0.78	0.01	1.02	0.086	11.04	537	0.001
Nd	0.752	0.66	0.09	12.00	0.063	9.4	432	0.002	0.77	0.02	2.03	0.137	17.9	94	0.012
Sm	0.754	0.83	0.08	10.57	0.107	12.9	326	0.003	0.84	0.08	11.11	0.226	27.0	79	0.011
Eu	0.77	0.74	0.03	4.52	0.059	8.03	1361	0.001	0.79	0.02	2.79	0.078	9.9	303	0.002
Gd	0.763	0.76	0.01	0.94	0.100	13.21	344	0.002	0.72	0.04	5.7	0.089	12.43	88	0.008
Tb	0.739	0.74	0.00	0.67	0.043	5.81	2172	0.000	0.84	0.10	14.0	0.061	7.22	577	0.001
Dy	0.746	0.72	0.02	3.06	0.043	6.0	530	0.002	0.81	0.07	9.23	0.068	8.41	139	0.003
Ho	0.749	0.72	0.03	4.40	0.057	8.01	2031	0.000	0.85	0.10	13.4	0.085	10.05	546	0.000
Er	0.74	0.75	0.01	1.10	0.064	8.49	685	0.001	0.81	0.07	9.7	0.050	6.10	185	0.003
Tm	0.732	0.67	0.06	7.81	0.042	6.22	2205	0.000	0.78	0.05	6.4	0.054	6.89	583	0.001
Yb	0.777	0.76	0.02	2.1	0.086	11.3	459	0.001	0.81	0.03	4.0	0.113	14.02	121	0.007
Lu	0.732	0.73	0.01	0.89	0.062	8.54	2084	0.000	0.80	0.06	8.7	0.043	5.45	555	0.001
Hf	0.711	0.74	0.03	3.95	0.036	4.92	590	0.001	0.77	0.05	7.7	0.137	17.88	170	0.005
Ta	0.808	0.75	0.06	7.24	0.043	5.75	2127	0.000	0.84	0.03	3.65	0.048	5.67	575	0.001
Pb	2.32	2.23	0.09	3.74	0.184	8.22	996	0.001	2.18	0.14	6.19	0.121	5.54	255	0.001
Th	0.748	0.77	0.02	2.76	0.041	5.34	1549	0.000	0.76	0.01	1.2	0.090	11.89	478	0.001
U	0.823	0.83	0.01	0.7	0.083	10.03	2098	0.000	0.82	0.00	0.45	0.072	8.8	539	0.000

	RV (μg g⁻¹)	20 μm AV (μg g⁻¹)	DIF (μg g⁻¹)	DIF% (%)	SD (1σ) (μg g⁻¹)	RSD (%)	Sensitivity (cps/μg g⁻¹)	DL (μg g⁻¹)	10 μm AV (μg g⁻¹)	DIF (μg g⁻¹)	DIF% (%)	SD (1σ) (μg g⁻¹)	RSD (%)	Sensitivity (cps/μg g⁻¹)	DL (μg g⁻¹)
Sc	0.74	3.26	2.52	340	0.613	18.81	108	0.004	3.78	3.04	411	0.495	13.09	64	0.008
Ti	3.61	*3.63*	*0.02*	*0.5*	*0.908*	*25.0*	*6*	*0.359*	*3.67*	*0.06*	*1.7*	*1.639*	*44.63*	*4*	*2.450*
V	1.01	1.05	0.04	4.1	0.125	11.9	127	0.002	0.94	0.07	7.36	0.246	26.30	74	0.015
Cr	1.19	*1.18*	*0.01*	*1*	*0.274*	*23.2*	*12*	*0.371*	*1.02*	*0.17*	*14*	*0.782*	*76.49*	*10*	*1.300*
Mn	1.42	1.37	0.05	4	0.128	9.39	131	0.013	1.6	0.2	12	0.695	43.66	77	0.070
Co	0.79	0.70	0.09	11.2	0.127	18.0	114	0.010	0.83	0.04	5.0	0.122	14.66	67	0.015
Ni	1.1	*1.15*	*0.05*	*5*	*0.313*	*27.1*	*21*	*0.454*	*1.01*	*0.09*	*9*	*0.616*	*61.29*	*13*	*0.838*
Zn	2.79	*2.88*	*0.09*	*3.30*	*0.427*	*14.8*	*7*	*0.532*	*2.40*	*0.39*	*14.07*	*1.115*	*46.52*	*3*	*4.396*
Rb	0.855	0.85	0.00	0.25	0.205	24.0	107	0.012	0.79	0.07	8.0	0.240	30.48	62	0.021
Sr	45.8	44.5	1.3	2.7	1.132	2.54	131	0.003	44.8	1.0	2.2	2.479	5.53	76	0.01
Y	0.79	0.87	0.08	10.47	0.117	13.4	133	0.007	0.94	0.15	18.46	0.346	37.02	79	0.013
Zr	0.848	0.94	0.09	10.97	0.107	11.4	75	0.014	1.06	0.21	25.07	0.116	10.96	42	0.030
Nb	0.824	0.87	0.04	5.4	0.114	13.1	145	0.003	0.84	0.02	1.85	0.274	32.63	88	0.012
Cs	0.664	0.55	0.11	17	0.208	37.5	165	0.017	*0.78*	*0.12*	*18*	*0.218*	*27.88*	*89*	*0.018*
Ba	3.2	3.17	0.03	1.0	0.296	9.36	20	0.036	3.17	0.03	0.9	0.226	7.11	12	0.096
La	0.72	0.72	0.00	0.4	0.060	8.4	159	0.003	0.82	0.10	13.8	0.121	14.77	92	0.010
Ce	0.813	0.71	0.10	12.9	0.090	12.77	181	0.002	0.72	0.09	11.2	0.101	13.95	108	0.006
Pr	0.768	0.78	0.01	1.2	0.035	4.5	205	0.002	0.84	0.07	9.6	0.122	14.52	117	0.006
Nd	0.752	0.62	0.14	18.1	0.141	22.9	31	0.068	0.66	0.09	12.0	0.172	25.98	18	0.099
Sm	0.754	0.78	0.02	2.8	0.349	45.0	26	0.066	0.57	0.18	23.97	0.541	87.78	15	0.359
Eu	0.77	0.87	0.10	13.3	0.183	21.0	103	0.008	0.72	0.05	6.2	0.269	37.27	60	0.013
Gd	0.763	0.87	0.10	13.71	0.247	28.4	27	0.060	0.90	0.14	18.15	0.387	42.88	16	0.165
Tb	0.739	0.82	0.08	11.41	0.179	21.8	175	0.005	0.93	0.20	26.43	0.140	15.02	103	0.007
Dy	0.746	0.81	0.07	8.95	0.131	16.1	43	0.020	0.90	0.15	20.24	0.150	16.71	24	0.041
Ho	0.749	0.89	0.14	18.93	0.099	11.09	160	0.004	0.89	0.14	18.89	0.114	12.85	95	0.010
Er	0.74	0.83	0.09	12.37	0.121	14.6	55	0.014	0.95	0.21	28.23	0.230	24.25	32	0.028
Tm	0.732	0.87	0.14	19.03	0.110	12.6	173	0.003	0.88	0.15	19.99	0.149	16.95	101	0.006
Yb	0.777	0.88	0.10	13.2	0.138	15.6	35	0.036	0.80	0.02	3.0	0.527	65.83	22	0.099
Lu	0.732	0.88	0.15	20.38	0.042	4.8	161	0.004	0.94	0.20	27.78	0.116	12.45	93	0.010
Hf	0.711	0.72	0.01	1.5	0.153	21.2	48	0.022	0.75	0.04	4.96	0.207	27.69	28	0.055
Ta	0.808	0.88	0.07	8.9	0.168	19.1	171	0.004	0.86	0.05	5.88	0.117	13.71	100	0.006
Pb	2.32	2.17	0.15	6.4	0.314	14.44	81	0.008	1.98	0.34	14.48	0.500	25.18	46	0.012
Th	0.748	0.83	0.08	10.4	0.095	11.49	130	0.005	0.81	0.07	8.80	0.160	19.68	78	0.014
U	0.823	0.79	0.03	3.9	0.055	7.01	177	0.004	0.75	0.08	9.5	0.058	7.80	104	0.008

RV: reference value of Jochum *et al.* (2011), AV: averaged value of analytical result, DIF: difference from reference value, DIF%: percentage of DIF against RV, SD: standard deviation of analytical values, RSD: relative standard deviation of analytical values, LD: lower limits of detection.

＊Values shown by Italic are reference values. Because of low background−signal count ratio, results of those elements were not determined in several sets, thus those values were extrapolated from other sets of analyses (*N*=5).
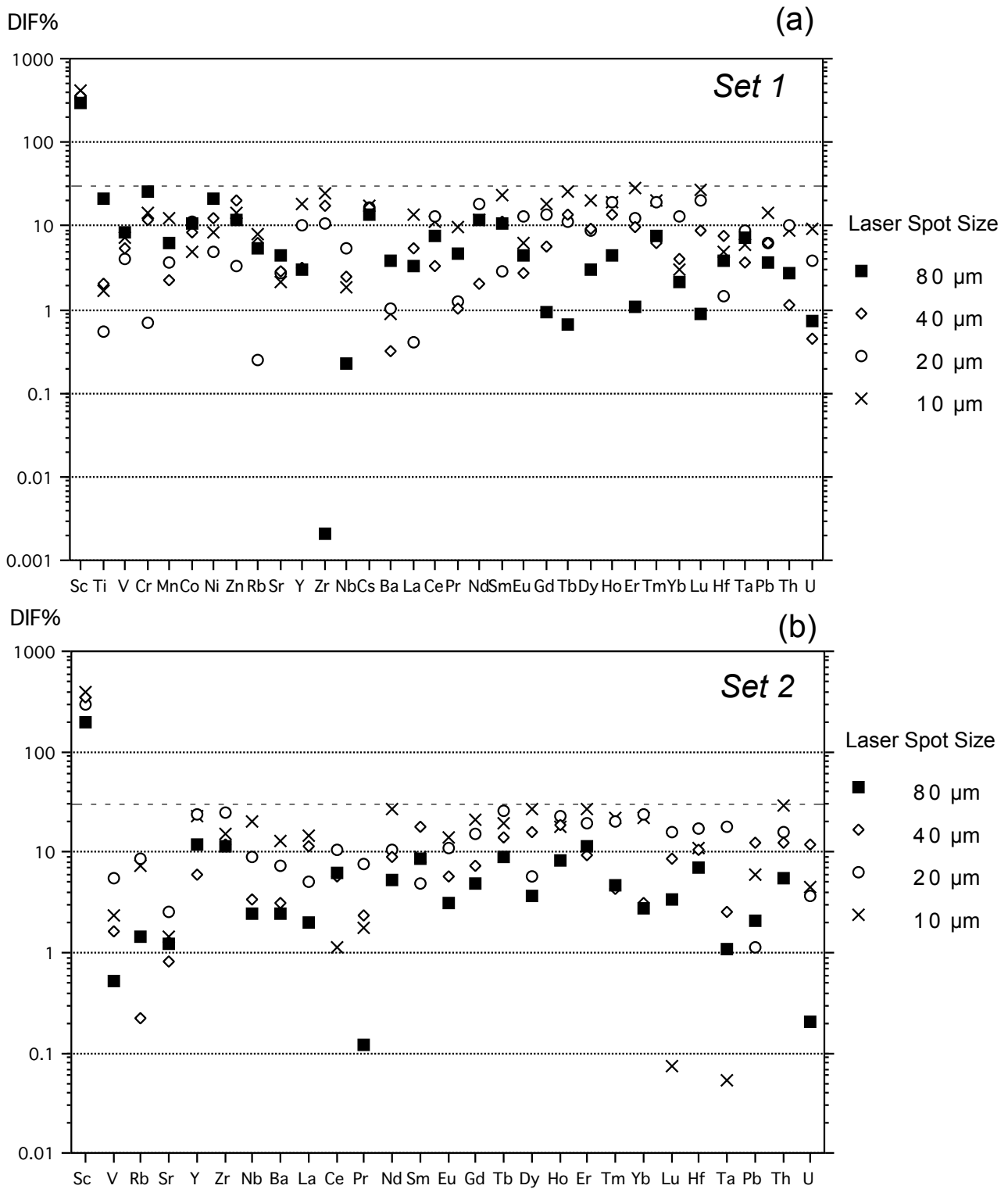
Fig. 6   DIF % of the Ca-normalized values determined for different pit diameters from the reference values of NIST 615 by Jochum *et al.* (2011). (a) Elemental Set 1 (34 elements) and (b) elemental Set 2 (27 elements). See text for detailed discussion.

Table 6 Quantitative results of replicate analyses (*N*=5) for NIST 615 determined using four pit diameters (80, 40, 20, and 10 μm) by elemental Set 2.

| | RV | 80 μm | | | | | | | 40 μm | | | | | | |
| | | AV | DIF | DIF% | SD (1σ) | RSD | Sensitivity | DL | AV | DIF | DIF% | SD (1σ) | RSD | Sensitivity | DL |
	(μg g⁻¹)	(μg g⁻¹)	(μg g⁻¹)	(%)	(μg g⁻¹)	(%)	(cps/μg g⁻¹)	(μg g⁻¹)	(μg g⁻¹)	(μg g⁻¹)	(%)	(μg g⁻¹)	(%)	(cps/μg g⁻¹)	(μg g⁻¹)
Sc	0.74	2.18	1.44	195	0.084	3.85	1318	0.001	3.30	2.56	347	0.191	5.77	307	0.001
V	1.01	1.02	0.01	0.53	0.042	4.15	1537	0.001	0.99	0.02	1.64	0.064	6.4	332	0.002
Rb	0.855	0.84	0.01	1.42	0.067	7.97	1579	0.001	0.86	0.00	0.2	0.041	4.8	288	0.001
Sr	45.8	46.4	0.6	1.22	1.608	3.47	1939	0.000	46.2	0.4	0.81	1.281	2.77	356	0.001
Y	0.79	0.89	0.10	12.05	0.029	3.31	1931	0.000	0.84	0.05	5.9	0.079	9.42	392	0.001
Zr	0.848	0.95	0.10	11.58	0.033	3.44	1017	0.001	0.95	0.10	12.2	0.084	8.83	202	0.002
Nb	0.824	0.80	0.02	2.42	0.042	5.19	2062	0.000	0.85	0.03	3.34	0.078	9.2	402	0.001
Ba	3.2	3.12	0.08	2.49	0.148	4.74	318	0.003	3.10	0.10	3.18	0.278	8.97	52	0.013
La	0.72	0.73	0.01	2.02	0.019	2.55	2432	0.000	0.80	0.08	11.34	0.051	6.39	429	0.001
Ce	0.813	0.76	0.05	6.4	0.035	4.57	2831	0.000	0.77	0.05	5.8	0.121	15.8	471	0.001
Pr	0.768	0.77	0.00	0.12	0.020	2.55	3063	0.000	0.75	0.02	2.32	0.083	11.05	532	0.001
Nd	0.752	0.79	0.04	5.38	0.080	10.14	501	0.002	0.82	0.07	8.9	0.097	11.9	87	0.010
Sm	0.754	0.82	0.06	8.56	0.107	13.09	416	0.002	0.89	0.14	18.0	0.168	18.92	73	0.015
Eu	0.77	0.79	0.02	3.10	0.023	2.95	1594	0.001	0.73	0.04	5.70	0.130	17.90	285	0.002
Gd	0.763	0.80	0.04	4.91	0.056	7.05	419	0.002	0.82	0.06	7.3	0.124	15.1	75	0.011
Tb	0.739	0.81	0.07	9.15	0.021	2.63	2693	0.000	0.84	0.11	14.3	0.076	9.04	498	0.001
Dy	0.746	0.77	0.03	3.7	0.030	3.92	658	0.001	0.86	0.12	15.6	0.092	10.68	119	0.004
Ho	0.749	0.81	0.06	8.21	0.012	1.51	2565	0.000	0.89	0.14	18.4	0.065	7.36	471	0.000
Er	0.74	0.83	0.09	11.51	0.057	6.85	859	0.001	0.81	0.07	9.5	0.115	14.2	161	0.003
Tm	0.732	0.77	0.03	4.72	0.023	3.05	2717	0.000	0.76	0.03	4.4	0.046	5.98	501	0.001
Yb	0.777	0.80	0.02	2.76	0.065	8.18	593	0.001	0.80	0.02	3.1	0.072	9.0	105	0.008
Lu	0.732	0.76	0.02	3.40	0.013	1.76	2623	0.000	0.80	0.06	8.8	0.045	5.63	465	0.001
Hf	0.711	0.76	0.05	6.99	0.044	5.82	762	0.001	0.79	0.08	10.8	0.094	11.94	141	0.005
Ta	0.808	0.80	0.01	1.10	0.023	2.86	2758	0.000	0.79	0.02	2.58	0.081	10.34	498	0.001
Pb	2.32	2.37	0.05	2.08	0.070	2.97	1323	0.001	2.03	0.29	12.61	0.173	8.52	238	0.001
Th	0.748	0.79	0.04	5.54	0.031	3.97	2177	0.000	0.84	0.09	12.40	0.039	4.61	384	0.001
U	0.823	0.82	0.00	0.21	0.032	3.91	2959	0.000	0.72	0.10	12.11	0.045	6.20	508	0.001

| | RV | 20 μm | | | | | | | 10 μm | | | | | | |
| | | AV | DIF | DIF% | SD (1σ) | RSD | Sensitivity | DL | AV | DIF | DIF% | SD (1σ) | RSD | Sensitivity | DL |
	(μg g⁻¹)	(μg g⁻¹)	(μg g⁻¹)	(%)	(μg g⁻¹)	(%)	(cps/μg g⁻¹)	(μg g⁻¹)	(μg g⁻¹)	(μg g⁻¹)	(%)	(μg g⁻¹)	(%)	(cps/μg g⁻¹)	(μg g⁻¹)
Sc	0.74	2.89	2.15	291	0.507	17.52	109	0.004	3.68	2.94	397	0.792	21.53	60	0.018
V	1.01	0.95	0.06	5.52	0.116	12.14	130	0.006	0.99	0.02	2.35	0.132	13.4	70	0.014
Rb	0.855	0.78	0.07	8.5	0.168	21.4	108	0.006	0.92	0.06	7.4	0.315	34.3	58	0.018
Sr	45.8	44.6	1.2	2.5	1.584	3.55	137	0.002	46.47	0.67	1.5	1.410	3.03	73	0.003
Y	0.79	0.98	0.19	23.82	0.107	10.9	136	0.005	0.97	0.18	22.79	0.211	21.8	73	0.014
Zr	0.848	1.06	0.21	24.42	0.118	11.2	73	0.014	0.98	0.13	15.51	0.288	29.4	39	0.024
Nb	0.824	0.90	0.07	9.0	0.164	18.3	150	0.006	0.99	0.17	20.45	0.173	17.5	81	0.014
Ba	3.2	2.97	0.23	7.2	0.648	21.8	21	0.037	2.79	0.41	12.8	0.764	27.4	11	0.076
La	0.72	0.76	0.04	5.2	0.044	5.8	156	0.005	0.82	0.10	14.4	0.153	18.6	85	0.010
Ce	0.813	0.73	0.09	10.7	0.115	15.8	182	0.003	0.82	0.01	1.1	0.294	35.8	99	0.006
Pr	0.768	0.71	0.06	7.6	0.117	16.4	202	0.003	0.78	0.01	1.8	0.100	12.81	103	0.009
Nd	0.752	0.67	0.08	10.47	0.348	51.7	34	0.054	0.96	0.20	27.2	0.169	17.7	16	0.146
Sm	0.754	0.79	0.04	5.0	0.226	28.5	26	0.083	0.82	0.07	8.94	0.386	47.0	14	0.140
Eu	0.77	0.69	0.08	10.8	0.093	13.5	106	0.008	0.66	0.11	13.8	0.234	35.3	54	0.020
Gd	0.763	0.88	0.12	15.1	0.304	34.6	29	0.062	0.92	0.16	20.79	0.452	49.0	14	0.105
Tb	0.739	0.93	0.19	25.54	0.162	17.4	180	0.003	0.89	0.15	19.76	0.172	19.47	92	0.010
Dy	0.746	0.79	0.04	5.76	0.234	29.6	43	0.016	0.95	0.20	27.06	0.128	13.5	22	0.067
Ho	0.749	0.92	0.17	22.71	0.127	13.8	167	0.004	0.88	0.13	17.60	0.156	17.7	85	0.010
Er	0.74	0.88	0.14	19.15	0.195	22.1	55	0.016	0.94	0.20	27.24	0.194	20.6	29	0.050
Tm	0.732	0.88	0.15	19.90	0.061	6.90	171	0.003	0.89	0.16	22.03	0.129	14.47	90	0.006
Yb	0.777	0.96	0.19	23.85	0.145	15.1	38	0.029	0.95	0.17	22.00	0.220	23.2	19	0.094
Lu	0.732	0.85	0.11	15.67	0.035	4.1	169	0.004	0.73	0.00	0.07	0.117	16.03	84	0.008
Hf	0.711	0.84	0.12	17.45	0.133	16.0	50	0.031	0.79	0.08	10.92	0.261	33.1	24	0.089
Ta	0.808	0.96	0.15	18.24	0.123	12.89	178	0.003	0.81	0.00	0.05	0.116	14.4	90	0.008
Pb	2.32	2.35	0.03	1.1	0.319	13.59	81	0.006	2.18	0.14	5.98	0.452	20.7	43	0.023
Th	0.748	0.87	0.12	16.01	0.060	6.88	131	0.004	0.96	0.21	28.66	0.136	14.12	70	0.010
U	0.823	0.85	0.03	3.7	0.129	15.10	174	0.003	0.79	0.04	4.4	0.193	24.50	98	0.005

RV: reference value of Jochum *et al.* (2011), AV: averaged value of analytical result, DIF: difference from reference value, DIF%: percentage of DIF against RV, SD: standard deviation of analytical values, RSD: relative standard deviation of analytical values, LD: lower limits of detection.

(2011) is shown in Fig. 6b. Accuracy were less than 30 % for all elements and all spot sizes, except for Sc, and the accuracy for most elements with 80 and 40 μm laser spot diameters was less than 20 %.

The estimated crater depth for analyses of Cpx, Amp, and Pl using the Set 2 program were Cpx 22 μm, Amp 16 μm, and Pl 16 μm for a laser spot diameter of 100 μm, Cpx 23 μm, Amp 16 μm, and Pl 16 μm for a 40 μm diameter, and Cpx 23 μm, Amp 15 μm, and Pl 16 μm for a 20 μm diameter. Thus, penetration would not occur during analyses of thin section samples with standard thickness (*ca.* 30 μm).

5. Conclusion

Analytical programs for trace element analysis of microspots in silicate minerals and glasses using LA-ICP-MS at GSJ-Lab were established. From evaluation of exhaustive basic data for He carrier gas flow rates and laser settings for ablation, appropriate instrumental operation settings were set as follows: 0.5 L min⁻¹ He carrier gas flow rate, 100 μm laser spot diameter,

5 Hz laser pulse repetition rate, and 40 % laser energy (fluence *ca*. 2.0 J cm^{-2}).

To evaluate precision and accuracy, NIST 615 and NIST 613 were analyzed as unknown samples. As a result, reproducibility as precision was mostly less than 30 % for 45 elements from ^{45}Sc to ^{238}U with laser spot diameters ranging from 100 to 10 μm. Accuracy was evaluated with respect to the DIFs between the analytical results and reference values by Jochum *et al*. (2011). Accuracy for analysis of NIST 613 was DIF < 30 %, except for Sc, Mn, Ni, and Ge. For NIST 615, the DIFs were less than 30 %, except for Tl with laser spot diameters of 20 μm and 10 μm, and Cd for a spot diameter of 20 μm. The crater depth for appropriate analytical conditions for Cpx, Amp, and Pl were estimated from confocal microscopy observations of craters ablated under given conditions, and it was confirmed that penetration of thin section samples with standard thickness (*ca*. 30 μm) did not occur with laser spot diameters of 100 – 20 μm.

For the general purpose of petrological and geochemical discussions, two suites of analytical programs (34 and 27 elements; Sets 1 and 2, respectively) were additionally prepared, and their accuracies were evaluated. The DIFs for the suite of 34 elements (Set 1) were mostly less than 30 %, although some (Cr, Mn, Ni, and Cs) with laser spot diameters < 40 μm exceeded 30 %. In the suite of 27 elements (Set 2), the DIFs were < 30 %, except for Sc.

Acknowledgement and author contributions

References

Chen, Z. (1999) Inter-element fractionation and correction in laser ablation inductively coupled plasma mass spectrometry. *Jour. Anal. Atom. Spectrom*., **14**, 1823–1828.

Date, A.R. and Gray, A.L. (1985) Plasma source mass spectrometry using an inductively coupled plasma and a high resolution quadrupole mass filter. *Analyst*, **106**, 1255–1267.

Eggins, S.M. and Shelley, J.M.G. (2002) Compositional

heterogeneity in NIST SRM 610-617 glasses. *Geostand. Newslett*., **26**, 269–286.

Eggins, S.M., Woodhead, J.D., Kinsley, L.P.J., Mortimer, G.E., Sylvester, P., McCulloch, M.T., Hergt, J.M. and Handler, M.R. (1997) A simple method for the precise determination of ≧ 40 trace elements in geological samples by ICPMS using enriched isotope internal standardisation. *Chem. Geol*., **134**, 31–326.

Eggins, S.M., Kinsley, L.P.J. and Shelley, J.M.G. (1998) Deposition and element fractionation processes during atmospheric pressure laser sampling for analysis by ICP-MS. *Appl. Surf. Sci*., **127–129**, 278–286.

Fryer, B.J., Jackson, S.E. and Longerich, H.P. (1995) The design, operation and role of the laser-ablation microprobe coupled with an inductively coupled plasma-mass spectrometer (LAM-ICP-MS) in the Earth sciences. *Can. Min*., **33**, 303–312.

Günther, D. and Heinrich, C.A. (1999) Enhanced sensitivity in laser ablation-ICP mass spectrometry using herium-argon mixtures as aerosol carrier. *Jour. Anal. Atom. Spectrom*., **14**, 1363–1368.

Günther, D., Jackson, S.E. and Longerich, H.P. (1999) Laser ablation and arc/spark solid sample introduction into inductively coupled plasma mass spectrometers. *Spectrochim. Acta B*, **54**, 381–409.

Hirata, T. and Kon, Y. (2008) Evaluation of the analytical capability of NIR femtsecond laser ablation-inductively coupled plasma mass spectrometry. *Anal. Sci*., **24**, 345–353.

Hirata, T., Shimizu, H., Akagi, T., Sawatari, H. and Masuda, A. (1988) Precise determination of rare earth elements in geological standard rocks by inductively coupled plasma mass spectrometry. *Anal. Sci*., **4**, 637–643.

Horn, I., Hinton, R.W., Jackson, S.E. and Longerich, H.P. (1997) Ultra-trace element analysis of NIST SRM 616 and 614 using lase ablation microprobe-inductively coupled plasma mass spectrometry (LAM-ICP-MS): A comparison with secondary ion mass spectrometry (SIMS). *Geostands. Newslett*., **21**, 191–203.

Houk, R.S., fassel, V.A., Flesch, G.D., Svec, H.J., Gray, A.L. and Taylor, C.E. (1980) Inductively coupled argon plasma as an ion-source for mass-spectrometric determination of trace-elements. *Anal. Chem*., **52**, 2283–2289.

Jackson, S.E. (2001) The application of Nd:YAG lasers in LA-ICP-MS. In Sylvester, P., ed., *Laser-ablation-ICP-MS in the Earth sciences – Principles and applications*. Mineralogical Association of Canada (Short Course Series Volume 29), 29–45.

Jackson, S.E. (2008) Calibration strategies for elemental analysis by LA-ICP-MS. *In* Sylvester, P., ed., *Laser-*

ablation-ICP-MS in the Earth sciences – Current Practices and Outstanding Issues. Mineralogical Association of Canada (Short Course Series Volume 40), 169–188.

Jochum, K.P., Weis, U., Stoll, B., Kuzmin, D., Yang, Q., Raczek, I., Jacob, D.E., Stracke, A., Birbaum, K., Frick, D.A., Günther, D. and Enzweiler, J. (2011) Determination of reference values for NIST SRM 610-617 glasses following ISO guidelines. *Geostand. Geoanal. Res.*, **35**, 397–429.

Kimura, J.-I., Takaku, Y. and Yoshida, T. (1996) Recent advancement of inductively coupled mass spectrometry (ICP-MS) and application to petrology. *Earth Sci.* (*Chikyu Kagaku*), **50**, 277–302 (in Japanese with English abstract).

Kimura, J.-I., Danhara, T. and Iwano, H. (2000) A preliminary report on trace element determinations in zircon and apatite crystals using excimer laser ablation-inductively coupled plasma mass spectrometry (ExLA-ICPMS). *Fission Track News Lett.*, **113**, 11–20.

Koch, J., Feldmann, I., Jakubowski, N. and Niemax, K. (2002) Elemental composition of laser ablation aerosol particles deposited in the transport tube to an ICP. *Spectrochim. Acta*, **B57**, 975–985.

Koch, J., von Bohlen, A., Hergenröder, R. and Niemax, K. (2004) Particle size distributions and compositions of aerosols produced by near-IR femto- and nanosecond laser ablation brass. *Jour. Anal. Atom. Spectrom.*, **19**, 267–272.

Kuhn, H.-R. and Günther, D. (2005) The agglomeration state of nano-second laser-generated aerosol particles entering the ICP. *Analyt. Bioanal. Chem.*, **383**, 434–441.

Kurosawa, M., Jackson, S.E. and Sueno, S. (2002) Trace element analysis of NIST SRM 614 and 616 glass reference materials by laser ablation microprobe-inductively coupled plasma-mass spectrometry. *Geostand. Newslett.*, **26**, 75–84.

Leichte, F.E., Meier, A. and Crock, J.G. (1987) Determination of the rare-earth elements in geological materials by inductively coupled mass spectrometry. *Anal. Chem.*, **59**, 1150–1157.

Longerich, H.P., Jackson, S.E. and Günther, D. (1996) Laser ablation inductively coupled plasma-mass spectrometric transient signal data acquisition and analyte concentration calculation. *Jour. Anal. Atom. Spectrom.*, **11**, 899–904.

Ludden, J.N., Feng, R., Gauthier, G. and Stix, J. (1995) Applications of LAM-ICP-MS analysis to minerals. *Can. Min.*, **33**, 419–434.

Mason, P.R.D. and Mank, A.J.G. (2001) Depth analysis by laser-ablation ICP-MS. *In* Sylvester, P., ed., *Laser-ablation-ICP-MS in the Earth sciences – Principles and applications*. Mineralogical Association of Canada (Short Course Series Volume 29), 63–81.

Mason, P.R.D., Jarvis, K.E., Downs, H. and Vannucci, R. (1999) Determination of incompatible trace elements in mantle clinopyroxenes by LA-ICP-MS: A comparison of analytical performance with established techniques. *Geostand. Newslett.*, **23**, 157–172.

Morishita, T., Ishida, Y., Arai, S. and Shirasaka, M. (2005) Determination of multiple trace element compositions in thin ($<$30 μm) layers of NIST SRM 614 and 616 using laser ablation-inductively coupled plasma-mass spectrometry (LA-ICP-MS). *Geostand. Geoanal. Res.*, **29**, 107–122.

Ogasawara, M. (2013a) Outline of shared research facilities of the Geological Survey of Japan. *GSJ Chishitsu News*, **2**, 65–66 (in Japanese).

Ogasawara, M. (2013b) Re-organization of shared research facilities of the Geological Survey of Japan after the great Earthquake. *GSJ Chishitsu News*, **2**, 69–73 (in Japanese).

Outridge, P.M., Doherty, W. and Gregoire, D.C. (1997) Ablative and transport fractionation of trace elements during laser sampling of glass and copper. *Spectrochim. Acta B*, **52**, 2093–2102.

Pearce, N.J.G., Perkins, W.T., Westgate, J.A., Gorton, M.P., Jackson, S.E., Neal, C.R. and Chenery, S.P. (1997) A compilation of new and published major and trace element data for NIST SRM 610 and NIST SRM 612 glass reference materials. *Geostand. Newslett.*, **21**, 115–144.

Perkins, W.T., Pearce, N.J.G. and Jefferies, T.E. (1993) Laser ablation inductively coupled plasma mass spectrometry: A new technique for the determination of trace and ultra-trace elements in silicates. *Geochim. Cosmochim. Acta*, **57**, 475–482.

Regnery, J., Stoll, B. and Jochum, K.P. (2010) High-resolution LA-ICP-MS for accurate determination of low abundances of K, Sc and other trace elements in geological samples. *Geostand. Geoanal. Res.*, **34**, 19–38.

Satoh, H., Ishiyama, D., Mizuta, T. and Ogata, T. (2001) Microanalyses of trace elements in mineral and rock samples by laser ablation inductively coupled plasma mass spectrometry (LA-ICP-MS). *Sci. Tech. Reps. Min. Coll. Akita Univ.*, **22**, 17–23 (in Japanese with English abstract).

レーザーアブレーション誘導結合プラズマ質量分析計（LA-ICP-MS）による
ケイ酸塩鉱物及びガラスのための微量元素分析

山崎 徹・山下康平・小笠原正継・斎藤元治

要 旨

　産業技術総合研究所　地質調査総合センター共同利用実験室（GSJ-Lab）設置の LA-ICP-MS により，珪酸塩鉱物及びガラスの微小領域の微量元素定量分析プログラムを構築した．検量線作成のための標準試料には，アメリカ国立標準技術研究所（NIST）の標準ガラス物質 (NIST 613 及び 611) を使用し，妥当な測定条件として He キャリアーガス流量 0.5 L min^{-1}，レーザーのスポット径 100 μm，パルスレート 5 Hz, エネルギー 40 %（fluence 〜 2.0 J cm^{-2}）を設定した．測定精度検証のため NIST 615 及び NIST 613 を未知試料として測定した結果，^{45}Sc から ^{238}U までの 45 元素について，レーザースポット径 100 μm – 10 μm において繰り返し測定精度（reproducibility；precision）はほぼ 30% 以下であった．標準試料の値からの差を示す確度（accuracy）は，NIST615 では Sc，Mn，Ni，Ge 以外の元素では，一般的に定量分析における精度の許容範囲の目安とされている < 30 % を下回り，NIST613 では，レーザースポット径 20 μm と 10 μm の Tl, 20 μm の Cd を除く全ての元素が 30 % 以下であった．天然の単斜輝石，角閃石及び斜長石を測定した際に想定されるレーザーピットの深さは，通常の岩石薄片試料において鉱物の掘り抜きは生じない程度であることが確認された．一般的な岩石学的，地球化学的議論に供するために 34 元素，27 元素を同時に測定可能な 2 つのセットをさらに作成し精度・確度を検証した結果，34 元素のセットではレーザースポット径 40 μm 以下の Cr，Mn，Ni，Cs において確度が 30 % を超えるものがいくつかあるが，その他は 30 % 以下であった．27 元素のセットでは，Sc を除き全てのレーザースポット径で確度は 30 % 以下であった．

地質調査総合センター研究資料集

地質調査総合センターの最新出版物

---

5 万分の 1 地質図幅	南部・北川・鴻巣・川俣・冠山	
20 万分の 1 地質図幅	静岡及び御前崎（第 2 版）・新潟（第 2 版）・横須賀（第 2 版）・大分（第 2 版）	
200 万分の 1 地質編集図	No. 4	日本地質図（第 5 版）
	No. 11	日本の火山（第 3 版）
特殊地質図	No. 40	関東平野中央部の地下地質情報とその応用
海洋地質図	No. 85	沖縄島北部周辺海域海洋地質図 （1:20 万）
	No. 86	室蘭沖表層堆積図 （1:20 万）
鉱物資源図	No. 7	南西諸島 （1:50 万）
構造図	No. 14	全国主要活断層活動確率地図
火山地質図	No. 18	蔵王火山地質図 （1:2.5 万）
	No. 19	九重火山地質図 （1:2.5 万）
水文環境図	No. 8	石狩平野 （札幌）
空中磁気図	No. 45	福井平野地域高分解能空中磁気異常図
	No. 46	養老断層地域高分解能空中磁気異常図
重力図	No. 30	徳島地域重力図 （ブーゲー異常）
	No. 31	京都地域重力図 （ブーゲー異常）
	S3	甲府地域重力構造図 （ブーゲー異常）
海外地球科学図	アジア地質図 （1:500 万）	
	中央アジア鉱物資源図 （1:300 万）	
	アジア鉱物資源図 （1:500 万）	
海陸シームレス地質図	S-4	海陸シームレス地質情報集「石狩低地帯南部沿岸域」
燃料資源図	FR-3	燃料資源地質図「関東地方」
土壌評価図	E-6	表層土壌評価基本図 「茨城県地域」
数値地質図	G-16	20 万分の 1 日本シームレス地質図　DVD 版
	G-17	九州地質ガイド
	GT-4	全国地熱ポテンシャルマップ
	S-2	海陸シームレス地質情報集「新潟沿岸域」
	S-3	海陸シームレス地質情報集「福岡沿岸域」
	V-3	口永良部島火山地質データベース
	P-2	日本重力データベース　DVD 版
	G20-1	20 万分の 1 数値地質図幅集「北海道北部」第 2 版
	G20-2	20 万分の 1 数値地質図幅集「北海道南部」第 2 版
その他	日本の熱水系アトラス	
	海と陸の地球化学図	

BULLETIN
OF THE
GEOLOGICAL SURVEY OF JAPAN

Vol. 66　No. 9/10　2015

CONTENTS

Geological Survey of Japan, AIST